Chemistry under high pressure

Maosheng Miao, [a,†] *Yuanhui Sun,*[a] *Eva Zurek*[b]*, Haiqing Lin*[c,d]

[a] *Department of Chemistry and Biochemistry, California State University Northridge, Northridge, California, 91330, USA*
[b] *Department of Chemistry, State University of New York at Buffalo, Buffalo, New York 14260-3000, USA*
[c] *Beijing Computational Science Research Centre, Beijing 100193, China*
[d] *Department of Physics, Beijing Normal University, Beijing, 100875, China*

[†] *email: mmiao@csun.edu*

Abstract Thanks to the development of experimental high-pressure techniques and methods for crystal structure prediction based on quantum mechanics, in the past decade numerous new compounds, mostly binary, with atypical compositions have been predicted, and some have been synthesized. Differing from conventional solid-state materials, many of these new compounds are comprised of various homonuclear chemical species such as dimers, trimers, pentagonal and heptagonal rings, polymeric chains, atomic layers and three-dimensional networks. Strikingly, it has been shown that pressure can alter the chemistry of an element by activating its (semi)core electrons, unoccupied orbitals and even the non-atom centered quantum orbitals located on the interstitial sites, leading to many new surprising phenomena. This Review provides a summary of atypical compounds that result from the effects of high-pressure either on the chemical bonds or the local orbitals. We describe various unusual chemical species and motifs, show how the chemical properties of the elements are altered under pressure, and illustrate how compound formation is favored even in situations in which chemical bonds are not formed. An extraordinary new picture of chemistry emerges as we piece together these unexpected high-pressure phenomena. In marked contrast to the previously held beliefs regarding the behavior of solids under pressure, we are learning that the quantum mechanical features of electrons, such as those that lead to the formation of directional bonds, inhomogeneous distributions of electrons and atoms, as well as variations in symmetry might be magnified under pressure. We discuss the influence of these phenomena on future studies that will probe chemistry at higher pressures, and explore more complex chemical compositions than those that have been studied to date.

[H1] Introduction

Many of us have been inspired by Jules Verne's 135-year old novel "Journey to the Center of the Earth" and amazed by the 2008 adapted film that pictorialized Verne's mind-boggling creatures and ancient species living in deep Earth caverns. Different to other Verne's novels, this story is purely fictional because Earth's interior is a place of extremely high pressures and temperatures. However, where this fantasy of paleontology ends is where the truth of chemistry begins. As we show in this Review, high pressure can greatly enrich the chemistry of matter by catalyzing the formation of many unusual chemical species and promoting many new phenomena that are just as stunning as the underground T-Rex and carnivorous plants, except this time they are real.

Although an actual journey to the center of the Earth is impossible, we can explore how matter changes under high pressure by performing laboratory experiments and computer simulations. Since Bridgeman proposed his first pressure sealing approach at 1905, the hydrostatic pressure that can be accessed in the laboratory has been increased from a few hundred atmospheres to 1000 GPa, especially thanks to the development of diamond anvil cell (DAC) techniques[1–5]. This has been accompanied by progress in many essential auxiliary techniques[6–10] that can accelerate chemical reactions (such as laser heating methods) or help to characterize the new compounds (such as X-ray and neutron scattering, IR and Raman spectroscopy). In contrast to experiments, computer simulations are fast and low-cost, and can go beyond the pressure limit of current techniques; therefore, they have often been at the forefront of the exploration of chemistry under pressure. Recently, crystal structure prediction (CSP) methods[11–25] based on first principles calculations (Box 1) have flourished owing to the dramatic advances in computer power and algorithmic development, providing scientists the tools to explore emergent chemical behavior under pressure. In the last decade, the structures and thermodynamic stabilities of numerous new compounds have been predicted without any experimental input, and some of the predicted compounds have been later verified by high-pressure experiments.

Various new phenomena have emerged as higher pressures have become attainable, and correspondingly the focus of high-pressure research has also progressed with time. Early investigations have been geared towards studying structural transitions[26–33], and changes in physical properties such as magnetism[34–36], metal–insulator transitions[37] and superconductivity[38–42], because these phenomena can occur at relatively low pressure. Although such studies remain an important part of mainstream research, the possibility to reach higher pressures has driven research into other areas. Of particular interest is the synthesis of atypical compounds — those with compositions different from 'textbook' stoichiometries that are common at atmospheric conditions. For example, instead of forming H_2S, H and S can yield an H_3S compound that is superconducting with a critical temperature, T_c, as high as 203 K under pressure[43–49]. Similarly, a large variety of atypical compounds, such as $NaCl_3$(Ref.[50]), LiN_5 (Refs [51,52]), LaH_{10} (Refs [53–58]), Fe_3Xe (Ref.[59]), CsF_3(Ref.[60]) and Na_2He (Ref.[61]) have been predicted or synthesized under high pressure. The discovery of a plethora of atypical compounds and their non-intuitive structural variations show how strikingly pressure can alter and enrich chemistry.

The progress achieved by simulations and experiments has led to the advancement of conceptual frameworks, including our understanding of how the behavior of matter changes under pressure. Together with Pauling's renowned rules of ionic crystal structures at atmospheric pressure[62], rules such as those put forward by Prewitt and Downs[63], by Grochala, Hoffmann, Feng and Ashcroft[64], and more recently by Zhang, Wang, Lv and Ma [6], can be used to rationalize the ways that structures, bonding features and electronic states change as pressure increases (Box 2). Many of the trends that emerge from experiments or computations agree with expectations of close-packing and homogeneity. For example, a large number of known compounds respond to pressure by becoming more homogeneous by compressing the longer and weaker bonds to a greater extend[63,64,6], assuming close-packed structures[63, 6], increasing their coordination numbers[63, 64], achieving higher symmetry[64] and delocalizing their electrons to an extent that eventually results in an insulator–metal transition[64, 6]. The propensity for electrons to attain homogenous charge distributions is caused by an effect rooted in quantum mechanics: the kinetic energy increases faster than the Coulomb energy with increasing electron density[65]. Because the

kinetic energy of the electrons can be minimized by adopting a homogeneous density distribution, electron delocalization and metallization appear to be the eventual fate of all matter under extreme pressures.

However, phenomena that cannot be intuitively understood have been observed. For example, not all matter becomes more homogeneous under pressure and deviation from close-packing of spheres may be used to achieve higher density[64]. It has been shown that many metals, such as Li and Na, abandon a close-packed geometry and adopt complex open structures accompanied by decreasing conductivity under high pressure[26,66]. Remarkably, experiments and theory are beginning to reveal that pressure may have a much more profound impact on the geometries and properties of atypical compounds than could have previously been imagined. These compounds often adopt quite surprising and unintuitive structures and bonding schemes. For example, in some classes of compounds electrons can become more localized, sometimes even detaching from all atoms and accumulating in the interstitial sites[67,68]. Moreover, the crystal phases observed under high-pressure are often non-homogeneous, with the most stable geometries containing many molecular or polymeric species[6,69], and coordination numbers are shown to decrease[60,70]. More strikingly, the repopulation of the atomic orbitals might significantly change the chemical behaviour of the atoms[60,71]. Thus, high-pressure chemistry becomes far more complex, with a large variety of compositions and structures being possible that often exhibit unpredictable properties. In addition, the chemical bonding in seemingly comparable materials such as $NaCl_3$ (Ref.[50]) and CsF_3 (Ref.[60]) can be very different.

In this Review, we show that the responses of the atomic orbitals and chemical bonds to increased pressure are key to classifying high-pressure compounds. Based on this framework, we describe a plethora of chemical species that contain homonuclear bonds, the reactivity of non-valence electrons and orbitals, the chemistry of non-atomic orbitals in electrides, and forces that drive compound formation without the creation of any local chemical bonds.

[H1] How pressure enriches chemistry

Most of the widely known inorganic compounds, such as NaCl, MgO and SiO_2 exhibit 'typical' compositions[72], which are primarily dictated by the 'typical' oxidation states of their constituent elements and by valence electrons and orbitals that determine the behavior of each element . Furthermore, heteronuclear bonds are often stronger than homonuclear bonds because charge transfer between different elements results in large binding energies. This effect is so strong for many strong oxidizing elements that at 1 atm only compounds with typical compositions are found. Any other composition would feature homonuclear bonds, which are less favourable. Interestingly, although typical compounds may adopt a wide variety of crystal structures, they often exhibit similar local structural features. For example, many oxides adopt structures consisting of tetrahedra or octahedra with non-oxygen atom at their centres. Nonetheless, plenty of compounds formed at ambient pressure have atypical compositions,[73] such as polyborides, polysulphides and polyphosphides, many of which are known as Zintl compounds.[74,75] Such compounds may form if the constituent elements are strongly inclined to cluster (for example, in the case of B, Si, S and P) or if the electronegativities of the constituent elements are not significantly different.

Knowing how the quantized states of electrons respond to reduced volume is the key to understanding the intricate and convoluted chemical phenomena that emerge under pressure. In this regard, we can classify the effects of pressure in two major categories: those that perturb the molecular orbitals and chemical bonds, and those that influence the atomic or other local orbitals. Both of these effects can lead to the formation of atypical compounds that exhibit new structural features and chemical properties (Figs 1 and 2). This rich chemistry not only alters the stoichiometries and geometries adopted by materials under pressure, but also drastically changes their physical properties, opening up new routes towards the design of novel materials with unique properties.

The strength of homonuclear bonds (whether they be diatomic, polyatomic or multicentered), relative to heteronuclear bonds, can be greatly enhanced under compression (Box 3). Pressure works against the interatomic repulsions and causes a decrease of the volume and the average interatomic distances. Consequently, the resonance integrals increase, resulting in a larger gap between bonding and antibonding states (Box 3), and stronger bonds. This effect is less significant for heteronuclear bonds, therefore pressure is expected to promote the formation of atypical compounds and structures that contain homonuclear bonds (Table 1 and Fig. 1), enriching chemistry in many ways. First, it enables the formation of a plethora of homonuclear clusters that do not exist at ambient conditions. Second, although some elements, such as B, might form many homonuclear species while reacting with various elements at 1 atm, pressure can cause the appearance of these species in one type of compounds formed with the same elements, as in the case of B species in compounds formed with Li[76,77]. Third, a large variety of homonuclear species may be found in different phases that emerge during the structural evolution of one compound with a fixed composition as a function of pressure.

Pressure has a pronounced effect on local orbitals and can lead to fascinating chemical phenomena that are not seen at atmospheric pressures. Pressure can change the difference in energies and the energy orderings of local quantum orbitals. The energies of all of the atomic orbitals generally increase with increasing pressure, just as one would expect for the particle in a box, because the electrons are more confined in the compressed solid. However, the energies of orbitals with lower principal quantum numbers and higher angular momenta, especially those having no corresponding core orbitals such as 2*p* and 3*d*, increase less significantly then the energies of orbitals with higher principal quantum numbers or lower angular momenta. As a result of this orbital energy reordering, the electrons are redistributed in different quantum orbitals under pressure. Although in many cases this redistribution of electronic charge leads to an increased delocalization, as well as an increased homogeneity of the electron density, in other cases, it does not. Therefore, the reordering of the energy levels is one of the main origins of the increasing inhomogeneity of electron density under pressure, as we discuss later in this article under heading ‘Chemistry of non-valence electrons and orbitals’.

Compounds featuring new homonuclear species

A large variety of atypical high-pressure compounds are formed from the enhancement of the strength or the number of homonuclear bonds. Many of the compounds that have been studied to date are binary, consisting of a metal (alkali, alkaline or transition metal) and a light element (H, B, C, N, O or F). Binaries containing heavier main group elements such as Cl, Si, Ge and S, have

also been studied, but to a somewhat lesser extent. One striking structural feature of these atypical compounds is that the anionic elements form various homonuclear species and moieties ranging from dimers, trimers, pentagonal and hexagonal rings, to polymeric chains, single and multiple layers and 3D networks (Table 1 and Fig. 1). The actual motifs that are formed in atypical compounds depend on the composition and pressure.

At atmospheric pressure, hydrogen forms typical compounds with the stoichiometry *M*H for the alkali metals, and MH_2 for the alkaline earth metals. The search for new hydrogen-rich materials was inspired by Ashcroft's prediction that the metallization pressure of hydrogen could be lowered through 'chemical pre-compression', which could be achieved by adding a dopant [78]. The resulting hydride would have all of the properties required to be a high-temperature superconductor at pressures that are currently accessible by DAC experiments[79,78]. Many metal hydrides with atypical compositions have been predicted to be stable (MH_n, *M*=Li, Na, K, Rb, Cs and $n > 1$; M=Mg, Ca, Sr, Ba and $n > 2$) and some have already been synthesized (for example, NaH_3 and NaH_7 (Ref.[80]), LiH_2 and LiH_6 (Ref.[81]), and CaH_4 (Ref. [82]). These compounds contain various H motifs, including molecular species such as H_2, linear and slightly bent H_3^- (Fig. 1Aa) (Ref [83–85]), triangular H_3^+(not in a metal hydride, Ref[86]), as well as extended species such as 1D helical chains (Ref.[87,88]) and 3D sodalite-like structures (Fig. 1Ab) (Refs [89,54–57]). They are comprised of electropositive elements, such as alkali, alkaline earth and rare earth metals, which donate their valence electrons to the new homonuclear hydrogenic sublattice. In contrast, high-pressure p-block hydrides (XH_n, *X*=Si, Ge, S, P etc)[11,42,43,90–98], do not always form polyhydride anions. Instead, they might form molecular, polymeric or 3D covalent moieties together with the p-block atoms that might become hypervalent. For example, in the record-breaking superconducting compound H_3S, each S atom is bonded to six H atoms, thereby sharing all of its six valence electrons, and each H atom is bonded in a linear fashion to two S atoms. Interestingly, the quantum nuclear motion of hydrogen atoms has crucial effects on stabilizing the high symmetry structures of H_3S[49] and LaH_{10}[99]. For example, density functional theory (DFT) calculations showed that the inclusion of nuclear quantum effects greatly lower the pressure of hydrogen symmetrization (H atoms located at the center between two neighboring S atoms) which is essential to explain the observed pressure dependence of T_c.[49].

The structural features found in hydrides under pressure influence their physical properties. For example, when the hydrogenic species satisfy electron counting schemes (for example, H_2, H^-, and H_3^-), and the electron transfer from the metal to the hydrogen atoms is complete, the corresponding compounds are insulators or semiconductors that can undergo pressure induced metallization[90]. If the polyhydrides contain molecular motifs with partially filled orbitals ($H_2^{\delta-}$) or extended lattices, such as hydrogenic 1D chains, 2D sheets, 3D cages, or *X*–H networks, the resulting compounds are metallic[90,100]. They are good candidates for high T_c superconductors and have been the focus of recent high pressure studies[90,100]. The first compound that broke the 25-year old world record of T_c set by the cuprates was found to be Im-3m H_3S, an atypical compound with a T_c of 203 K near 150 GPa[45]. DFT-based CSP predicted the presence of 3D hydrogenic lattices in a number of hydrides including CaH_6 (Ref.[89]), YH_{10} (Refs[56,101]) and LaH_{10} (Refs[54,56]). In these phases, hydrogen atoms form a clathrate-like lattice with the metal atoms sitting in the center of the cages (Ref.[102]). DFT calculations have found these clathrate-like species to be superconductors with very high T_c within the Bardeen–Cooper–Schrieffer (BCS) mechanism.[100,103] In BCS theory, superconductivity is due to the pairing of the electrons

mediated by nuclear vibrations (phonons). A higher T_c can be expected if a material exhibits high phonon frequencies, strong electron–phonon coupling interactions, and a high electron density at the Fermi energy, all of which can be found in H_3S and the superhydrides. These theoretical predictions inspired the high-pressure synthesis of Fm-3m LaH_{10} (Refs [53,55,57,58]). Two independent groups measured astonishingly high T_c values of 250–260 K at pressures of 170–200 GPa in this compound[55,57].

Because of its deficiency of electrons, the metalloid element B has a tendency to form clusters thereby sharing its electrons through multicentered bonds. In binary compounds formed at ambient pressure, especially with metal atoms, a large variety of B moieties can be found (Refs [72,73,104]). These include isolated B anions in Mn_4B, B_2 dimers in Cr_5B_3, zig–zag chains in FeB, double chains in Cr_3B_4, 2D covalent networks in MgB_2 and CrB_2, and 3D covalent networks in LaB_4, LaB_6, and YB_{12} (Ref.[104]). Because B–B bonds are strong, these types of materials usually exhibit exceptional mechanical strength, especially when combined with the high electron density of transition metals. For this reason, numerous transition metal borides, such as FeB_4 (Ref.[105]), ZrB_4 (Refs[106]), WB_4 (Refs[107]), ZrB_3 (Refs[108,109]), Rh_2B (Ref.[110]) and RhB_2 (Refs[110,111]) have been proposed and studied as superhard materials. Metal compounds such as MgB_2, which feature B covalent networks, may exhibit superconducting properties owing to the light atomic mass of B and strong B–B bonds[112]. Interestingly, mechanical strength and superconductivity can both be found in FeB_4 (Refs[113,114]). This compound was first predicted by DFT calculations to be stable at 0 GPa,[113] but was only synthesized under pressure (8 GPa).[114] High pressure greatly enriches the structural varieties observed in the borides. It stabilizes many compounds with a large variety of compositions and a plethora of B motifs that are otherwise not stable at atmospheric conditions. For example, in predicted and synthesized Li–B compounds[115–117,76,77,118,119], B can be found as an anion in Li_6B (Ref.[76]), a dimer in Li_4B (Fig. 1Ba) (Ref[76]), a chain in Li_2B (Fig. 1Bb) and LiB (Refs[76,116,119]) and a graphene-like layer in LiB (Fig. 1Be) (Refs[116,119]) and Li_3B_2 (Ref.[76]). Calculations also showed that B can form ribbons (Fig. 1Bd) in a B-rich compound MgB_6 under pressure.[120] Moreover, with increasing pressure, boron lattices evolve from graphane-like layers, to interconnected B_4 layers, to B_4 chains (Fig. 1Bc) and finally to graphene-like planar layers at very high pressure in FeB_4 compounds, as predicted by DFT[105].

Carbon is the most versatile element; it can exist in numerous allotropes and form different bonding motifs in organic molecules. In contrast, C adopts a much smaller variety of motifs in metal compounds at ambient pressure, although some metal carbides can crystallize in various compositions and contain a number of different moieties.[72] Pressure greatly enhances the variety of carbon-based motifs that can be found in many atypical compounds, ranging from those featuring C_2^{2-} in CaC_2 (Fig. 1Ca) (Refs[121–124]), C_2^{4-} in ThC_2 (Ref.[125]), C_3^{4-} in Mg_2C_3 (Fig. 1Cb),[126] hexagonal rings (Fig. 1Cc)[123], polymeric chains[121,122,125,127,128], and nanoribbons (Fig. 1Cd)[121–123,125,128,129], to different layered forms such as graphene (Fig. 1Ce)[125,128,130], graphane and multi-layers[131]. Moreover, DFT calculations have shown that the carbon sublattices in some metal carbides, such as YC_2 (Ref.[128]) and CaC_2 (Ref.[121]), progressively evolve from single atoms to 3D covalent networks with increasing pressure for a given stoichiometry.

Under ambient conditions, the most well-known metal nitrides are comprised of N in a −III oxidation state. Nevertheless, many other nitrogen-containing species[72] can be found including those that contain azide (N_3^-)[132] or pernitride (N_2^{2-})[133] anions, transition metal interstitial nitrides

and, in some metastable compounds, pentazenium (N_5^+) and petazolate (N_5^-) ions[134–136]. Pressure can greatly enrich the chemistry of binary nitrides by promoting the formation of N–N bonds and polynitrogen species either in new atypical compounds or in compounds of already known compositions. This behavior has been widely exploited to predict and synthesize nitrogen-based high energy density materials. For example, an ultra-incompressible and very hard rhenium nitride pernitride [$Re_2(N_2)(N)_2$], which contains an N_2^{4-} anion, has been synthesized under high pressure and persists under ambient conditions[137]. Other polynitrogen species have been found in synthesized nitrogen compounds under pressure, such as $[N_2]^{2-}$ in FeN_2 (Ref.[138]), N zig–zag chains in FeN_4 (Ref.[138]), $[N_4]^{4-}$ in Mg_2N_4 (Fig. 1Db) (Ref.[139]), and N–N chains in MgN_4 (Ref.[139]), along with the large variety of N clusters that have been predicted that includes [N_3^{4-}(Fig. 1Da), N_2^{2-}, N_4^{4-}, N_6^{4-} ring (Fig. 1Dd), and polymeric chains] in various Mn–N compounds[140,141]. Furthermore, new polynitrogen species might also emerge in the structural evolution of a compound under pressure; one example is the planar triadius star-like N_4 species in FeN_2 that has been predicted at pressures higher than 228 GPa (Ref.[142]). Among all the polynitrogen species, the pentazolate anion (N_5^-) is the most striking (Fig. 1Dc)[143]. In contrast to the extreme difficulty of obtaining the N_5^- ring under atmospheric conditions, many computational and experimental studies have shown that N_5^- becomes thermodynamically stable and common under pressure, in compounds such as LiN_5 (Fig. 1Dc) (Refs [51,52,134]), NaN_5 (Ref.[144]), CsN_5(Ref.[145]), MgN_{10}(Ref.[140]) and CuN_5 (Ref.[146]). When the pressure is lowered, some of these compounds can be recovered in experiments,[147] thus providing a new route to obtain N_5^- based high energy density materials.[148]

Because O is a strong oxidizing element, it tends to assume an oxidation number of −II. However, $O_2^-$and O_2^{2-} have been found in various metal superoxides and peroxides at 1 atm, although many of them are only metastable.[72] External pressure does not promote the formation of more O-based chemical species, probably because the large number of electrons prevents the formation of polyatomic species. However, pressure does promote the formation of O_2^{2-}. For example, an O rich Fe compound, FeO_2 (Fig. 1Ea), becomes stable at pressures similar to those reached in Earth's lower mantle, as revealed by recent calculations and experiments, which suggested a new oxygen cycling mechanism in Earth's interior[149–153]. This compound assumes a very simple structure in which the centers of O_2^{2-} species occupy an face-centered cubic (FCC) lattice and forms a cubic NaCl type structure with Fe^{2+} ions.

Halogen atoms usually assume a typical oxidation number of −I and form stoichiometric compounds with metals at ambient conditions. Although assorted trihalide and multihalide anions have been studied at atmospheric pressures,[154] most of them are not thermodynamically stable with rare exceptions such as I_3^- (Ref.[155]). Recently, computations have shown that pressure could be a promising method to stabilize multi-halides. For example, F_3^- can exist in a stable CsF_3 compound in the pressure range from 15 to 30 GPa.[60] When the pressure is higher than 30 GPa, the F_3^- anion decomposes and the released F oxidizes the core electrons of Cs. In a more recent work, both F_3^- (Fig. 1Fa) and F_5^- (Fig. 1Fb) have been found in CsF_3 and CsF_5 under pressure.[156] Similarly, Cl_3^- anions can exist in Na–Cl (Fig. 1G) (Ref.[50]) and K–Cl (Ref.[157]) compounds with high Cl compositions. However, the more common forms of Cl in these compounds are 3D covalent networks[50,158].

Different to low-*Z* oxidant elements, many heavier elements can adopt a wide composition range, and their crystal lattices can contain a plethora of complex moieties under ambient conditions. For example, Si can form various compounds with alkali and alkaline earth metals, such as MSi (M=Li, Na, K, Rb, Cs, Ca, Sr, Ba), M_2Si (M=Mg, Ca, Sr, Ba) and MSi_2 (M=Ca, Sr, Ba).[72] Many Si species are already known such as $[Si_4]^{4-}$ tetragons in NaSi (Refs [159–162]) and zig–zag Si chains in BaSi (Ref.[163]). However, as shown by many DFT predictions, pressure creates new Si based species that have not been observed at ambient conditions, such as Si squares in Ca–Si (Fig. 1H) (Ref.[164]), as well as Si layers and cages in Cs–Si (Ref.[165]).

[H1] Chemistry of non-valence electrons and orbitals

The changes in the chemical behavior and properties of the elements that are caused by the reordering of atomic orbital energies under pressure are particularly fascinating. For example, at sufficiently high pressures, Ni can theoretically become an insulator[166], and K and Cs have been observed to behave like transition metals because of the pressure-induced $s \rightarrow d$ electronic charge transfer[167–169]. Moreover, calculations showed that xenon oxides of various compositions become thermodynamically stable under pressure[170–174], and Fe can become a strong oxidant and oxidize Xe to form stable compounds[59]. Remarkably, pressure can also promote compound formation between elements that do not react under ambient conditions. For example, Li and Be were predicted to form stable Li–Be compounds including LiBe, Li_3Be, $LiBe_2$ and $LiBe_4$, at pressures higher than 15 GPa (Ref.[175]). The atypical compounds that result from the change of the chemical behavior of an element are fundamentally different to those resulting from the formation of homonuclear bonds. These compounds do not contain homonuclear clusters and their atypical compositions are associated with changes in oxidation states and coordination numbers (Fig. 2).

[H2] Reactivity of core electrons

One of the most remarkable phenomena that can occur under high pressure is the activation of core electrons.[176] The atomic shell structure and the Pauli exclusion principle suggest that the properties of the elements are determined by the (valence) electrons in their outermost shells and that the inner shell electrons and high-lying unoccupied orbitals are not involved in chemical bond formation. Thus, the chemical behaviour of a particular element, including the oxidation states it can adopt, are dictated by its location in the periodic table. For many years, it was believed that an element cannot react further if it loses all of its valence electrons or gains enough electrons to completely fill its valence orbitals.

The discovery of the reactivity of the noble gases, which was inspired by Pauling's theoretical prediction[177] and realized by Neil Bartlett's eminent synthesis of $XePtF_6$ (Ref.[178]), disproved the belief that an element with a complete valence shell is not reactive. Since then, hundreds of compounds of noble gases, including Xe, Kr and Ar, have been synthesized. Most of them feature chemical bonds involving the valence electrons of the noble gases.[179] Another successful example of activating a closed shell is the synthesis of HgF_4 in a noble gas matrix under very low temperatures,[180] which was inspired by quantum chemical predictions that included correlation and relativistic effects.[181,182] However, only the 5*d* subshell participates in the reaction, and the produced HgF_4 molecules are unstable and have very short life-times even at a low temperature

of 4 K. The oxidation of Cs^+ in SO_2 and CH_3CN solution using an electrochemical method is the only reported attempt to date to alter the reactivity of core electrons[183]. However, it was later shown that this result is invalid[184], and the activation of inner-shell electrons in chemical reactions still remains elusive.

One of the key questions of chemistry, "can core electrons participate in chemical bond formation?", was first answered at high pressures. Hydrostatic pressure can steadily shift the orbital energies of the atoms (see Fig. 3a, Box 3 and Ref.[185]), forcing the atoms to change the oxidation states they can assume. A first principles CSP study based on the PSO algorithm revealed that even moderately high pressures could coerce the formation of atypical CsF_n (n>1) compounds[60]. For example, CsF_2 was predicted to become stable at only 5 GPa; CsF_3 and CsF_5 were predicted to become stable at 15 GPa and 50 GPa, respectively, and remained stable up to at least 200 GPa . What makes the CsF_n compounds so special is the origin of their atypical composition. Different to the systems discussed in the previous section, which were stabilized by the formation of homonuclear bonds, the stability of CsF_n arises from the activation of the Cs 5*p* electrons, meaning that their energy becomes higher than that of the F 2*p* electrons (Fig. 3a). Indeed, the calculated Bader charges revealed a continuous increase of charge on the Cs atoms for increasing *n* (Fig. 3b), which can only be explained by the activation of the 5*p* core electrons. The involvement of the Cs 5*p* electrons can be directly seen in the projected density of states (PDOS) plots that show a large amount of 5*p* states both below and above the Fermi level (Fig. 3c).

The activation of the 5*p* electrons completely alters the chemistry of Cs, leading to very unusual structural and bonding features in the CsF_n compounds[60]. CsF is a prototypical compound that transforms from rock-salt structure to CsCl structure at 5GPa (Fig. 2Aa). In CsF_n (n>1) compounds the coordination number of Cs dramatically decreases, due to the formation of various discrete species such as CsF_2 molecules in CsF_2 (Fig. 2Ab) CsF_2^+ ions in CsF_3,(Fig. 2Ac) and CsF_5 molecules in CsF_5 (Fig. 2Ae). A later theoretical work[156] on the Cs–F system revealed that CsF_4 can also be stable under high pressure with Cs being present in a mixed valence state, consisting both of Cs^{III+} (in the form of CsF_2^+) and Cs^{V+} (in the form of CsF_5). Both CsF_2 and CsF_2^+ are linear (Figs. 2Ab and 2Ac). At 100 GPa, the shortest Cs–F bond length is 2.015 Å (Ref.[60]), close to the Xe–F bond length previously observed in XeF_2(Ref. [186]); whereas CsF_5 is planar pentagonal (Fig. 2Ae), corresponding to a AX_5E_2 structure in the valence-shell electron-pair repulsion (VSEPR) model[72].This structure has been found experimentally in $[XeF_5]^-$ (Ref. [187]), a species that is isoelectronic with the CsF_5 molecule. The Cs–F bonds involving Cs 5*p* electrons are covalent, as elucidated by the crystal orbital Hamiltonian populations (COHP)[188] and the electron localization functions (ELF)[189] (Fig. 3d). Both methods revealed covalent bonds in the unusual CsF_n (n=2,3,5) compounds, with bond strengths that are comparable to those found in Xe–F systems. Inspired by the prediction of high pressure CsF_n compounds, metastable chemical species containing Cs in high oxidation states, such as CsF_2^+, CsF_5 (Ref.[190]) and $[CsO_4]^+$ (Ref.[191]) were also predicted using quantum chemistry calculations. The CsF_n compounds are fundamentally different to many other alkali polyhalides. Taking $NaCl_3$ as an example,[50] its unusual composition results from the enhancement of the Cl–Cl bond strength and the formation of Cl–Cl dimers under pressure (Fig. 3e). In $NaCl_3$, the oxidation state of Na remains +I, whereas in CsF_3, Cs is in +III state.[60]

Calculations have also revealed that the activation of the semicore 5*d* electrons of Hg by pressure causes the formation of atypical HgF_n (n=3 and 4) compounds (Figs 2Ba and 2Bb)[70]. In contrast to the short-lived HgF_4 molecules in a noble gas matrix [180], first principles calculations predicted that HgF_4 in the solid phase becomes thermodynamically stable at 38 GPa. The structure obtained from CSP consists of stacks of HgF_4 rectangular molecules (Fig. 2Bb). The electronic structure of solid HgF_4 clearly reveals that Hg assumes a +IV oxidation state and forms moderately strong covalent bonds with four neighboring F atoms, which can only happen when two 5*d* electrons are involved (Fig. 3f). The remaining 5*d* electrons form a d^8 configuration and fill the four lower *d* states in a planar rectangular field, causing a gap of 0.71 eV (as computed with the Heyd–Scuseria–Ernzerhof density functional) at 50 GPa.[70] When the pressure is higher than 73 GPa, the simulations showed that Hg can also form a stable HgF_3 compound in which Hg is in a +III oxidation state. When the pressure is higher than 200 GPa, HgF_4 is predicted to become unstable and decompose into HgF_3 and F_2. This result is very striking considering that HgF_3 is actually metallic because Hg is in a d^9 configuration while losing one 5*d* electron to F. The singly occupied d^9 state is not stable because of the high DOS at the Fermi level and it becomes spin polarized, making HgF_3 a rare example of a 5*d* ferromagnetic material (Fig. 3f)[70]. Similar to Cs–F compounds, the coordination numbers of Hg in HgF_n are high in the strongly ionic compounds HgF_2 and HgF_3, but they plunge to 4 in HgF_4 owing to the formation of strong Hg–F covalent bonds involving 5*d* semicore electrons.

[H2] Reactivity of unoccupied non-valence orbitals

Under high pressure, the unoccupied non-valence orbitals can also be activated and play an essential role in an element's chemistry. When this occurs, many remarkable chemical phenomena might appear: noble gas elements can become oxidants and assume a negative charge[192]; halogens and chalcogens can be reduced beyond their typical oxidations states of −I and −II[193]; and alkali metals can become anions with charges beyond 1− [71] . CSP performed with the PSO algorithm coupled with DFT revealed that Xe, Kr and Ar could form stable compounds with Mg at 125, 250, and 250 GPa, respectively[192]. Two later computational works predicted the formation of stable Li_nAr (Ref.[194]) and Li_nXe (Ref.[195]). In these compounds the noble gas elements were found to be negatively charged, and the extra electrons to occupy the outer *d* shell orbitals of the noble gas atoms (5*d* for Xe, 4*d* for Kr and 3*d* for Ar). Because the energies of the *d* orbitals increase less significantly compared to those of the *s* and *p* orbitals under pressure, the outer shell *d* orbitals become lower in energy than the 3*s* and 3*p* orbitals of Mg (Box3), causing a large charge transfer from Mg to the noble gas atoms (Fig. 4a and b). Strikingly, some compounds with higher Mg compositions such as Mg_2Xe behave like high pressure electrides (Fig. 4a) at pressures much lower than expected for elementary Mg[192,196], a phenomenon that has also been seen in other alkali or alkaline earth compounds such as Na_3Cl[50].

Another surprising phenomenon is that alkali and alkaline earth metals might be reduced and become anions under pressure[71]. Although systems containing Na^-, K^-, Rb^- and Cs^- have been synthetized[197] and predicted[198] at 1 atm, alkali metal anions with negative charges below −1 have not yet been observed. The reasons why alkali metals become anions at high pressure are different than those leading to the same phenomena at 1 atm. Consider, for example, the Li_nCs (n=1–5) compounds that have been predicted to be stable at pressures higher than 100 GPa (Ref.[71]). DFT calculations revealed charge transfer from Li to Cs, resulting in Cs anions with

charges as large as −1.58 (Li_5Cs at 150 GPa). The structural evolution of compounds that involve the unoccupied non-valence orbitals in bonding, such as Li_nCs and Mg_nXe_m, is distinctly different to those formed because of the activation of core electrons. In contrast to Cs in CsF_n compounds, the coordination number of Cs increases from 8 in LiCs, to 10 in Li_2Cs, to 12 in Li_3Cs and then decreases to 11 in Li_4Cs and Li_5Cs. The non-monotonous change of the coordination number is likely a result of the enhancement of the Li–Li bond strength under elevated pressure.

If pressure can cause the reduction of noble-gas atoms, it may also cause the further reduction of a halogen anion, since X^- is isoelectronic to a noble gas. Computations have revealed this phenomenon in Na_nCl (Ref.[50]) and Li_nI (Ref.[193]). At a pressure greater than 20 GPa, the calculated Bader charge on I was found to be as large as −2.8 in Li_nI, indicating a nominal oxidation state of −4 or −5. Similar to Cs in Li_nCs compounds, the charge of I goes beyond -1 because the occupation of the 5*d* orbitals increases under pressure as their energies increase less significantly compared with other orbitals such as Li 2*s* and 2*p* . The relative downshift of the 5*d* and 6*p* orbitals has a significant effect on the 5*d* transition metals. Although many late 5*d* transition metals such as Pt and Au are known to act as anions in compounds such as CsAu (Ref.[199]) and Cs_2Pt (Ref.[200]) because of strong relativistic effects, pressure can further extend their unusual oxidation states. DFT calculations predicted that, under high pressure, the negatively charged states of Au could stretch beyond −III in Li_nAu (n=1–6) compounds[201], and Ir can be stabilized in a −III state in the K_3Ir compound at pressures above 10 GPa (Ref.[202]).

[H1] Chemistry of non-atom-centered orbitals

Like in "Journey to the center of the Earth", whenever we think we have seen the most striking phenomena in chemistry, high pressures surprise us with another totally unexpected new wonder. High-pressure electrides (HPEs) are one such example. An electride is a type of material in which some of the electrons detach from the atoms and occupy the empty interstitial sites[203–205]. In these materials, the electrons themselves play the role of the anions, hence the name electrides. One of the first known examples of elemental compounds presenting electron density maximization at the interstitial sites under high pressure is Cs-IV. [206–208]. Therefore, it was dubbed cesium electride.[209] The cesium atoms in this non-close packed phase have a coordination of eight and more interstitial space with respect to Cs atoms in Cs-II and Cs-III phases. Similar electronic distributions have been computed for hypothetical structures of Na and Li under high pressure[210,211]. The localization of electrons in the interstitial sites under pressure was also demonstrated in a model system consisting of a lattice of impenetrable spheres[212]. The well-recognized explicit suggestion and observation of HPE were from a joint theoretical and experimental work showing that Na, a prototypical metal, could become a transparent insulator at pressures higher than 200 GPa (Refs[67,209,210]). Moreover, experiments and theory demonstrated that Li transforms into a semiconductor HPE with a gap of 0.3 eV at 80 GPa (Refs [215–220]).

Electrides are known to form at atmospheric conditions and hundreds of electride compounds have been discovered since the 1980s[203–205]. However, the formation of electrides requires the presence of empty sites that can accommodate electrons and implies a volume increase. Therefore, it was quite a surprise that simple metals, such as Cs, Na and Li, were found to become electrides under high pressure.[67,215] Moreover, many other examples of HPEs were later

predicted using DFT, including Mg (Ref.[196]), Al (Ref.[221]) and even C (Ref.[222]). Besides elementary solids, some compounds with excess metal compositions, such as Mg_3O_2 (Ref.[223]) and Mg_2Xe (Fig. 4a)[192], are also predicted to be stable and become HPEs at high pressure. Several mechanisms have been proposed to explain the electride formation including *s–p*, *p–d* and *s–d* electron redistributions[67,196,210], multicenter bond formation[224,225], and change in the symmetry, electron count, and band crossing [226]. We will focus on a simple mechanism based on the concept of quasi-atoms that can directly explain and roughly predict the formation of HPEs without the performance of DFT calculations.

To understand the formation of HPEs, we must first realize that the interstitial space in a crystalline lattice does not merely add room for electron redistribution among atomic orbitals, it can also accommodate quantum orbitals that can be occupied by electrons.[68] These orbitals are analogous to those in hydrogen-like atoms and can be approximated by the quantum mechanical solutions of an infinite spherical well, that is why the vacant sites in HPEs are termed interstitial quasi-atoms (ISQs)[68]. At atmospheric conditions, the energies of atom-centered valence orbitals are lower than the ISQ orbital. Under pressure, the energies of many valence atomic orbitals increase more quickly and become destabilized relative to the 1*s* orbital of the ISQ because of the strong repulsion from core electrons (Fig. 5a). If the energy gain from transferring electrons into ISQ orbitals is sufficient, the material will adopt an open structure and become an electride.

The quasi-atom concept enables us to directly determine the likelihood that an element will form an HPE. This propensity can be estimated semi-quantitatively by comparing the pressure dependence of the ISQ 1*s* orbital energy to the energies of atomic orbitals using a He matrix model (Fig. 5b). For example, the energies of the valence orbitals of Li and Na become higher than those in an ISQ orbital at about 80 GPa (Fig. 5c), in agreement with DFT and DAC results showing that Li and Na can form HPEs at relatively low pressures.[67,215,216,227] Other elements such as Mg, Al, and C require much higher pressures (Fig. 5c). Moreover, the quasi-atom model showed that the energies of some *d* orbitals decrease with respect to those of the ISQ as pressure increases (Fig. 5d)[68] and when these are valence orbitals, they might prevent the formation of HPEs. This simple mechanism counteracting HPE formation causes many remarkable phenomena. For example, K and Cs are more reactive than Na and Li, therefore they should form HPEs at even lower pressures. Cs-IV, stable between 4.3–12 GPa (Ref.[168]), is an HPE, the electronic structure of which has traditionally been explained by an $s \rightarrow d$ electronic transition[228]. Although not explicitly stated, the earlier calculations imply that the charge density of Cs-IV can be reproduced by placing an *s* orbital on the interstitial sites where the ISQs are centered[207]. At higher pressures, the electrons are transferred from the ISQ back to the *d* orbitals of this alkali metal. Similarly, although Mg_2Xe was computed to be an HPE at 125GPa — the lowest pressure at which this compound is stable — (Fig. 4a), an ISQ → Xe 5*d* charge donation occurs at higher pressures, until the ISQ totally disappears (Fig. 4c)[192].

ISQs do not only assume the role of anions in compounds. Computations have shown that they can form all types of chemical bonds, including ionic, metallic and covalent with other atoms and, more interestingly, with other ISQs (Fig. 5e)[229]. The formation of ISQ–ISQ covalent bonds turns out to be the key to the gap between the conduction and valence bands in Li HPE.[230] Different to compressed Na, which has a gap of 1.3 eV at 200 GPa (Ref.[67]), Li is a semiconductor with a mere gap of less than 0.3 eV (Refs[215,227]). The structure of Li HPE was

only resolved using CSP several years after the phase was discovered in a DAC experiment[215,220,227]. In contrast to Na HPE, Li HPE consists of two sets of ISQs with a formula of $Li_{20}E^{II}_8E^{I}_4$ (Ref.[220]) in which E^{II} and E^{I} are doubly and singly occupied ISQs. The presence of E^{I} should make Li HPE metallic, which is in contrast to what is observed in DAC experiments and DFT calculations[215,220,227]. However, E^{I} ISQs always appear in pairs with a distance of about 1.3 Å between them (Fig. 5f) [230], indicating that they form covalent bonds. The crystal wavefunctions at the Γ point clearly show the bonding and the antibonding states of the E^{I}–E^{I} bonds (Fig. 5g)[230]. The energy splitting of the two states is the origin of the semiconducting gap of Li HPE (Ref.[230]).

An ISQ behaves very much like a chemical element. We therefore may add an ISQ to the periodic table under pressure and place it above He. Although an ISQ is not a physical entity, it represents an undividable species that has unique chemistry. The periodic table is not a collection of physical entities, but rather of elementary chemical species, which is why all the isotopes are considered as a single chemical element in the table. In that sense, an ISQ is required to complete the periodic table under pressure.

[H1] Chemistry without chemical bonds

Another remarkable phenomenon that has been observed under pressure is that chemical reactions can occur despite the fact that no chemical bonds are formed. In this last tale of our journey, quantum mechanics is not the determining factor, but it sets the stage. The quantization of the electronic states in atoms sets two energies — the ionization energy and the electron affinity — which are essential to the chemical properties of an element. For some elements, especially light noble gasses such as He, the gap between these two energies is very large and inhibits the formation of any chemical bonds. Thus, except for very rare cases such as the insertion into the large empty sites in clathrates or cage molecules,[231] the bonding with O inside strong electric fields or the ferroelectric molecular cavity formed by strongly polar molecules,[232] and the formation of ionic species such as HHe^{+},[233] He is almost inert.

Pressure cannot alter the tenacious inertness of He, because the relevant orbitals (1*s*, 2*s* and 2*p*) are insensitive to compression. Thus, it was quite a surprise when experiments and theory showed that He can react and form stable compounds with Na under high pressure[61]. The enthalpy of formation of this Na_2He compound was computed to be ~0.35 eV/atom at 350 GPa, indicating a large chemical driving force that goes way beyond any weak interactions. However, all of the computational tools used to probe and categorize chemical interactions between atoms in solids, such as Bader charges, PDOS, ELF and COHP, provided no evidence for chemical bonding between He and its neighboring atoms[61,234,235]. Thus, paradoxically, it appeared that He reacts with Na under high pressure while keeping its chemical inertness.[234] This raises the question: what is the driving force that leads to the formation of the Na_2He compound under high pressure?

The clue that helped unravel the stabilization mechanism was hidden in the electronic structure of Na_2He (Refs[234–236]). This compound is actually an electride and its chemical formula can be written as Na_2EHe (Ref.[61]), where E represents an ISQ with a nominal charge of 2−. Therefore, the actual reaction is between He and an ionic compound $(Na^{+})_2E^{2-}$. A one-dimensional ionic

crystal model can be used to illustrate this mechanism (Fig. 6Aa and 6Ba).[235] For ionic crystals with the formula AB, the inserted He atoms have no place to go except for between a cation and its neighboring anion, thereby increasing the electrostatic potential energy (Madelung energy in crystals). Such a reaction is therefore not favored. In contrast, for an ionic compound with the formula AB_2 (or equally A_2B), the inserted He atoms can be placed between the two neighboring anions (or cations), which decreases the Madelung energy. This effect becomes stronger under high pressure because the ions get closer, improving the driving force for the He insertion. In 3D crystals such as MgO and MgF_2, the mechanism of He-insertion becomes more subtle. As shown by DFT and PSO simulations, although MgO adopts the rock-salt structure that resembles alternating AB ionic chains in a 3D crystal (Fig. 6Ab), the inserted He atoms do not go directly in between the Mg and O ions[235]. Instead, they are located out of the Mg–O plane in a perturbed structure (Fig. 6Ac and 6Ad). This structural distortion prevents the unfavored separation of Mg and O ions at the cost of an increased volume. In contrast, He atoms in MgF_2He are located between the F atoms in a crystal structure that resembles the AB_2He chains (Fig. 6Bc and 6Bd)[235]. The deviation from the 1D ionic chain structure in MgF_2 avoids the direct contact of F ions, but again at the price of a larger volume, which is unfavorable under increasing pressure (Fig. 6Bb).

A similar He insertion reaction can occur, in principle, in many ionic compounds with unequal numbers of cations and anions. Before this mechanism was proposed, He insertions into various ionic compounds have been theoretically predicted in systems such as Na_2O (Ref.[61]), Na_2S, K_2S (Ref.[237]) and even H_2O (Ref.[238]). To test the Madelung energy hypothesis, calculations were performed on the insertion of He into prototypical AB compounds (LiF and MgO), as well as A_2B and AB_2 compounds (Li_2O and MgF_2) (Fig 6Ca and Cb)[235]. Because these ionic materials are comprised of hard-core ions, one can single out the electrostatic energy change owing to He insertion under pressure. The large driving forces favoring compound formation caused by the change of Madelung energies are clearly shown for AB_2 and A_2B compounds, but not for AB compounds (Figs. 6Cc and 6Cd). Equally important, the insertion of He into AB_2 or A_2B compounds also leads to a considerable decrease of the PV term of the enthalpy[235]. This effect is caused by the increased volume of the AB_2 or A_2B compounds owing to the strong repulsions between neighboring ions of the same type, which is relieved by the insertion of He (Figs. 6Bb - 6Bd). The volume effect hinders, instead, the insertion of He into AB type compounds such as MgO (Figs. 6Ab - Ad). Furthermore, counteracting effects such as the occupation of higher lying orbitals play a role during the He insertion reactions in compounds consisting of polarizable ions such as CaF_2 and K_2S, leaving only a narrow pressure window in which the He inserted compounds are stable[235,237]. A more recent theoretical study has shown that He insertion can happen in crystals comprised of polarized molecules such as ammonia under pressure. In this case, the mechanism is more subtle: the insertion lowers the Madelung energy by reorienting the NH_3 molecules[239], although the behavior of NH_3 is different in pristine ammonia that has been predicted to become ammonium amide ionic solid at 90 GPa[240].

He insertion reactions are not only an example of unintuitive chemistry, but they also yield compounds with interesting properties and suggest that He may be present in larger amounts than previously thought in rocky planets. A recent theoretical work has shown that H_2O–He compounds exhibit superionic phenomena[241], that is to say that He and H^+ may diffuse in a liquid-like state in the solid lattices formed by O^{2-} ions. Many minerals in the Earth's interior are

comprised of an unequal number of cations and anions, suggesting that they might host a considerable amount of He. This remarkable reactivity of He under pressure might be key in solving the supply shortage of He that is bound to happen in the near future because He is light and escapes into space. For example, calculations showed that He could potentially be inserted into FeO_2 and form stable FeO_2He compounds at the pressure conditions close to the mantle–core boundary (>120 GPa)(Ref.[242]), indicating a large storage of He in that region.

The electrostatic driving force is not limited to He insertion reactions. Such an effect should drive many other reactions that involve the rearrangement of highly charged or polarized atoms. However, most of the reactions involve large charge transfer among the reactants and the formation or destruction of various chemical bonds. The change of the Madelung energy is either included in these strong chemical interactions or is dwarfed by them; therefore, it is not the determining factor for these chemical reactions regardless of the pressure.

[H1] Future directions and challenges

Despite the tremendous progress in high-pressure studies during the past decades, we are still at the beginning of a long journey and many new discoveries will continuously surprise us. We can nevertheless project the current progress to a future that embraces higher pressures, more complex substances, such as ternary and quaternary compounds, and the quenching and application of some of these new materials to ambient conditions.

First, high-pressure experiments and simulations will continue to discover new atypical compounds in the pressure range that is commonly accessible by current experimental techniques (< 200 GPa). Many binary materials have already been studied, but there are numerous ternary, quaternary and more complex systems that are awaiting to be predicted or synthesized. For reasons similar to those that can be used to explain the large variety of homonuclear species present in atypical binary compounds under pressure, many ternary or quaternary compounds with more complicated species (homonuclear or heteronuclear) may also be stable. Furthermore, many new atypical compounds involving orbitals that are unoccupied at 1 atm, or those that are centered on interstitial sites are expected to be stable at pressures lower than 200 GPa. Some of them may contain heavy elements with strong spin–orbit interactions and could potentially behave as new topological insulators, Weyl metals, strongly correlated materials and non-BCS superconductors.

The access to higher pressures, especially above 200 GPa, will open a new territory of high-pressure chemistry. As the pressure increases to 500 GPa or 1 TPa, the atoms come close enough so their core electrons are activated, making ‘core chemistry’ increasingly important. In this regime, elements will transform and behave as new chemical species. For example, most of the alkali and alkaline earth elements (such as Cs, Rb, K, Ra, Ba and Sr) might behave like p-block elements, because the electrons filling inner *p* orbitals can be activated. Some p-block elements, especially those with higher *Z* (such as Pb, Bi, In, Sn and Te), might behave like transition metals because their filled *d*-shells become involved in forming chemical bonds with neighboring atoms. It is expected that core chemistry will be essential to the properties of materials under extremely high pressures and temperatures that are present at the conditions of the interiors of large extraterrestrial planets.

We should not forget that high-pressure techniques are becoming indispensable to obtain new materials with unusual properties. These techniques can complement more conventional synthesis approaches to discover new materials. It is important to develop methods that can be used to quench the materials to low or ambient pressures. This can be achieved by increasing the kinetic barriers towards decomposition and/or inducing chemical pressure. The latter can be created when an atom or ion is located at a crystalline site that is smaller than the atomic or ionic radius.[243] For example, we may apply high pressure method to synthesize new electride materials. These materials usually have atypical compositions because they consist of additional alkali and alkaline earth metals that can provide an excess number of electrons. Because high pressure is an effective method to stabilize atypical compounds, it can be used to greatly increase the chemical space for new electride materials. Furthermore, as shown in several cases, the insertion of other elements that can increase the size of interstitial spaces will promote the formation of electrides, because it lowers the 1*s* orbital energies of ISQs. This suggests that we may greatly improve our chances to find electride materials in ternary compounds under moderate pressures, and recover them at ambient conditions.

High-pressure experiments, computer simulations and data science will need to work together and overcome many challenges to successfully undertake future studies. It is also crucial to develop an understanding of how chemical bonding and reactivity change under pressure. The general propensity of increased homogeneity under pressure and its effects on the structures and properties of materials dominated high-pressure studies for the last several decades. However, the numerous recent discoveries of new compounds with atypical compositions show that homogeneity may decrease under pressure. The quantum mechanical features of electrons (directional bonds, inhomogeneous charge distribution, low symmetry) might be magnified by pressure. Indeed, it is the enhanced tendency to form homonuclear bonds and the reordering of the energies of various quantum orbitals (atomic and non-atomic) that leads to the formation of a plethora of new chemical species, with a large variation of oxidation states. These trends and many other high-pressure effects might play important roles in complex materials such as ternary and quaternary compounds, leading to a boundless treasure trove of new materials and phenomena. The exploration of this new world of chemistry has just begun.

Acknowledgements M.M. and Y.S. acknowledge the support of NSF CAREER award 1848141, and computational resources provided by XSEDE (TG-DMR130005). M.M. also acknowledges the support of ACS PRF 50249-UNI6. E. Z. acknowledges the support of NSF (DMR-1827815), and DOE (DE-SC0020340). H.L. acknowledges financial support from NSAF U1930402 and computational resources from the Beijing Computational Science Research Center.

Competing financial interests The authors declare no competing financial interest.

Author contributions:
M.M. conceived the synopsis of the article, proposed the conceptual framework and wrote the first draft. M.M. and E.Z. made major revisions to the article. E.Z. wrote Box1 and made major contributions to the section on hydrides. Y.S. made Table 1, Figure 1, contributed to the literature search and helped with other figures. H.L. supported and discussed the research and writing.

[H1] ToC blurb:

High pressure leads to striking new chemistry. Many new compounds with atypical compositions and a plethora of novel chemical species can be stabilized by the formation of homonulcear bonds and of the activation of core electrons, non-valence and non-atomic orbitals.

Table 1: Representative chemical-species/structural-motifs found in high-pressure atypical compounds

Element	Structural Motif	Compound	Structure	Homonuclear bond length (Å)	Pressure (GPa)	Ref.
Motifs formed by homonuclear bonds						
Hydrogen	H_2	NaH_3	Cmcm	0.755 (50 GPa)	50	[80]
	Linear and bent H_3^- (Fig. 1Aa)	CsH_3	Cmmm	0.961 (50 GPa)	30–200	[84]
	H_3^+	H_5Cl	Cc	0.870 (300 GPa)	100–300	[86]
	1D helical chain	SrH_6	$R\bar{3}m$	1.033 (250 GPa)	250	[87]
	3D cage (Fig. 1Ab)	CaH_6	$Im\bar{3}m$	1.238 (150 GPa)	50–200	[89]
		LaH_{10}	$Fm\bar{3}m$	1.068–1.157 (300 GPa)	200–300	[54,56]
Boron	B anion	Li_6B	$R\bar{3}m$	--	100–200	[76]
	B dimers (Fig. 1Ba)	Li_4B	C2/m	1.631 (50 GPa)	50	[76]
	B icosahedron	B_6O	--	--	4–5.5 (exp.)	[244]
	B chains (Fig. 1Bb)	Li_2B	Cmcm	1.646 (100 GPa)	50–100	[76]
	B_4 cluster–chains (Fig. 1Bc)	FeB_4	I4/m	1.599 (500 GPa)	100–542	[105]
	B ribbons (Fig. 1Bd)	MgB_6	Cmcm	1.742 (18 GPa)	0–18.3	[120]
	Graphene-like layers (Fig. 1Be)	LiB	$P6_3/mmc$	1.761 (50 GPa)	1–70	[76]
	3D covalent B network	FeB_4	Imma	1.499–1.596 (600 GPa)	542–1000	[105]
			Immm	1.684-1.917 (0 GPa)	0	[113]
Carbon	C_2^{2-} (Fig. 1Ca)	CaC_2	C2/m	1.258 (0 GPa)	0–0.5	[122]
	C_2^{4-}	ThC_2	C2/c	1.330 (1 atm)	0–3	[125]
	C_3^{4-} (Fig. 1Cb)	Mg_2C_3	Pnnm	1.330 (1 GPa)	0–5.8	[126]
	C hexagonal rings (Fig. 1Cc)	Y_2C_3	Fmmm	1.497 (50 GPa)	32–137	[123]
	C polymer chains	CaC_2	Cmcm	1.400–1.460 (16 GPa)	0–16	[121]
			Cmcm	1.394–1.452 (4 GPa)	0.5–15.2	[122]
	C nanoribbons (Fig. 1Cd)	CaC_2	Immm	1.468–1.516 (15.2 GPa)	15.2–105.8	[122]
			Immm	1.480–1.550 (20 GPa)	16–20	[121]
	Graphene (Fig. 1Ce)	YC_2	P6/mmm	1.434 (300 GPa)	267–300	[128]
	C multi-layers	C_3N	R3m	1.509–1.572 (1 atm)	15.4–100	[131]
Nitrogen	N_2^{4-} anion	ReN_2	$P2_1/c$	1.412 (1 atm)	1 atm	[137]
	$[N_2]^{2-}$	FeN_2	Pnnm	1.307 (58.5 GPa)	58.5 (exp.)	[138]
	N zig–zag chains	FeN_4	$P\bar{1}$	1.291–1.303 (135 GPa)	135 (exp.)	[138]
	$[N_4]^{4-}$	Mg_2N_4	$P2_1/n$	1.303–1.339 (58.5 GPa)	58.5 (exp.)	[139]
	N–N chain	MgN_4	Ibam	1.311–1.325 (58.5 GPa)	58.5 (exp.)	[139]
	planar triadius N_4	FeN_2	$P6_3/mcm$	1.250 (228 GPa)	228	[142]
	N_3^- anion	LiN_3	C2/m	1.199 (1 atm)	0–60 (exp.)	[132]
		CsN_3	I4/mcm	1.199 (0 GPa)	0–6	[136]
	N_3^{4-} anion (Fig. 1Da)	Mg_2N_3	Imm2	1.428 (0 GPa)	37–100	[141]
			Pmmn	1.371 (50 GPa)	33–126	[140]

	N_2^{2-} anion	MgN_2	Cmcm	1.260 (5 GPa)	5–40	[141]
		PtN_2	$Pa\bar{3}$	1.410 (1 atm)	50 (exp.)	[133]
	N_4^{4-} anion (Fig. 1Db)	MgN_2	$P6_3/mcm$	1.351 (0 GPa)	40–100	[141]
	N_5^- rings (Fig. 1Dc)	LiN_5	$P2_1/m$	1.300 (20 GPa)	10–100	[51]
			$P2_1/c$	1.286–1.305 (50 GPa)	15–50	[52]
	N_6^{4-} rings (Fig. 1Dd)	MgN_3	$P\bar{1}$	1.393 (0 GPa)	80–100	[141]
Oxygen	O_2^{2-} (Fig. 1Ea)	FeO_2	$Pa\bar{3}$	1.756 (76 GPa)	76 (exp.)	[150]
	O_2^- (Fig. 1Eb)	NaO_2	Immm	1.317 (5 GPa)	0–20	[245]
Fluorine	F_3^- (Fig. 1Fa)	CsF_3	C2/m	1.739 (0 GPa)	15–30	[60]
			$R\bar{3}m$	1.742 (0 GPa)	0–30	[156]
	F_5^- (Fig. 1Fb)	CsF_5	C2/c	1.299 (10 GPa)	4–21	[156]
Chlorine	Cl_3^- (Fig. 1G)	$NaCl_3$	Pnma	--	18–60 (exp.)	[50]
			Pnma	2.804 (40 GPa)	20–48	[50]
Silicon	Si_4 tetragon	NaSi	C2/c	2.376–2.403 (0 GPa)	1 atm	[246]
	Si square (Fig. 1H)	CaSi	I4/mmm	2.107 (20 GPa)	12–50	[164]
	Zig–zag Si chain	BaSi	Imma	2.309 (20 GPa)	6–65	[163]
	Si layer	$CsSi_6$	$Im\bar{3}m$	2.361 (1 atm)	0–8.4	[165]
	Si cage	$CsSi_6$	C2/m	2.435–2.560 (0 GPa)	20.8–30	[165]
Motifs resulting from the participation of core electrons and non-valence outer orbitals						
Cs (5*p* core electrons)	Cs–F_8 cube (Fig. 2Aa)	CsF	$Pm\bar{3}m$	3.206 (0 GPa)	5–200	[60]
	CsF_2 (Fig. 2Ab)	CsF_2	I4/mmm	2.358 (20 GPa)	5–17	[60]
	CsF_2^+ (Fig. 2Ac)	CsF_3	C2/m	2.015 (100 GPa)	30–200	[60]
	CsF_5 (Fig. 2Ae)	CsF_5	Fdd2	1.886–1.957 (150 GPa)	50–200	[60]
Hg (5*d* semi-core electrons)	Hg–F_8 cube (Fig. 2Ba)	HgF_3	$Fm\bar{3}m$	2.181–2.519 (100 GPa)	73–500	[70]
	HgF_4 (Fig. 2Bb)	HgF_4	I4/m	1.949–2.532 (50 GPa)	73–200	[70]
Cs (5*d* non-valence orbitals)	Cs–Li8 cube (Fig. 2Ca)	LiCs	$Pm\bar{3}m$	2.396 (150 GPa)	150 - 200	[71]
	Cs–Li_{10} dodecahedrons (Fig. 2Cb)	Li_2Cs	I4/mmm	2.086–2.233 (150 GPa)	Metastable 100–200	[71]
	Cs–Li_{12} icosahedrons (Fig. 2Cc)	Li_3Cs	Pnna	2.200 (150 GPa)	150–200	[71]
	Cs–Li_{11} tri-capped cube (Fig. 2Cd)	Li_4Cs	C2/m	2.120–2.330 (150 GPa)	150	[71]
	Cs–Li_{11} tri-capped cube (Fig. 2Ce)	Li_5Cs	P2/m	2.120–2.330 (150 GPa)	100–150	[71]

725

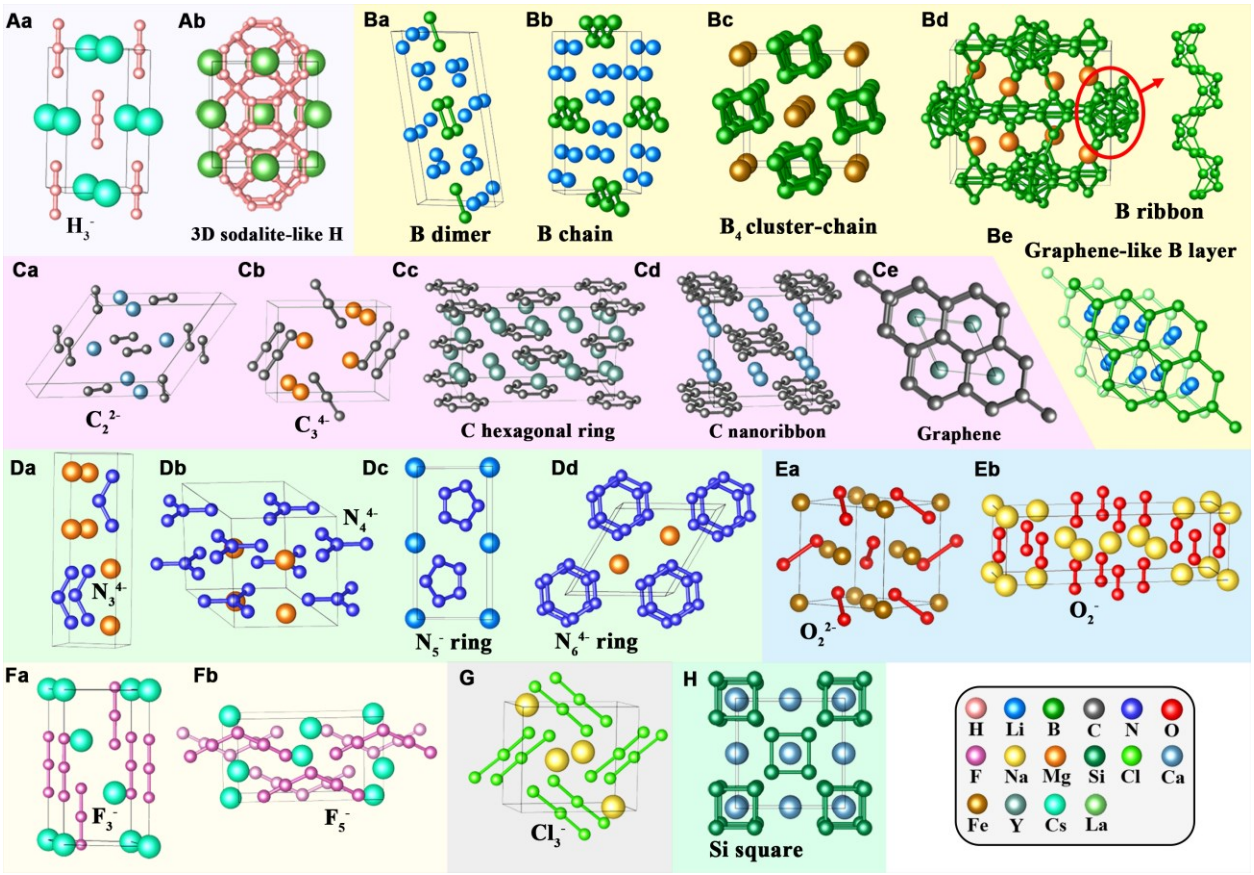

Figure 1. Selected homonuclear species present in atypical high-pressure compounds. A| Hydrogen homonuclear species, including H_3^- in CsH_3 (Ref.[84]) (part **Aa**) and 3D sodalite-like H in LaH_{10} (Refs[54,56]) (part **Ab**). LaH_{10} was predicted to be stable between 200 – 300 GPa (Refs[54,56]). **B|** Boron homonuclear species, including B dimers in Li_4B (Ref.[76]) (part **Ba**), B chains in Li_2B (Ref.[76]) (part **Bb**), B_4 cluster–chains in FeB_4 (Ref.[105]) (part **Bc**), B ribbons in MgB_6 (Ref.[120]) (part **Bd**), and graphene-like B layers in LiB (Ref.[76]) (part **Be**). **C|** Carbon homonuclear species, including C_2^{2-} in CaC_2 (Ref.[122]) (part **Ca**), C_3^{4-} in Mg_2C_3 (Ref.[126]) (part **Cb**), C hexagonal rings in Y_2C_3 (Ref.[123]) (part **Cc**), C nanoribbons in CaC_2 (Ref.[122]) (part **Cd**), and graphene in YC_2 (Ref.[128]) (part **Ce**). **D|** Nitrogen homonuclear species, including N_3^{4-} in Mg_2N_3 (Ref.[141]) (part **Da**), N_4^{4-} in MgN_2 (Ref.[141]) (part **Db**), N_5^- rings in LiN_5 (Ref.[51]) (part **Dc**), and N_6^{4-} rings in MgN_3 (Ref.[141]) (part **Dd**). LiN_5 has been predicted to be stable between 10 – 100 GPa by DFT[51,52] and has been synthesized by DAC experiments at 45 – 72 GPa.[147] **E|** Oxygen homonuclear species, including O_2^{2-} in FeO_2 (Refs[149,150]) (part **Ea**), and O_2^- in NaO_2 (Ref.[245]) (part **Eb**). **F|** Fluorine homonuclear species, including F_3^- in CsF_3 (Refs[60,156]) (part **Fa**), and F_5^- in CsF_5 (Ref.[156]) (part **Fb**). **G|** Chlorine homonuclear species, such as Cl_3^- in $NaCl_3$ (Ref.[50]). **H|** Silicon homonuclear species such as Si squares in CaSi (Ref.[164]). Details on structures, stable pressures and bond lengths for each motif and compound are reported in Table 1.

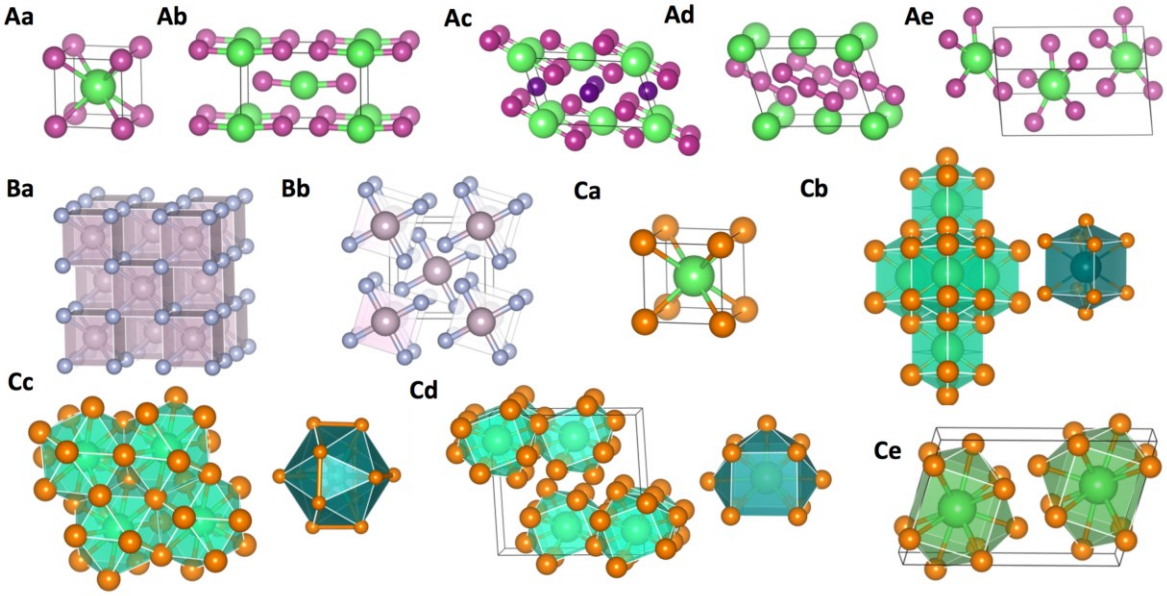

Figure 2. Predicted structural evolution of compounds formed via the involvement of non-valence electrons and orbitals under pressure. A| Structures of CsF_n (n =1–5) compounds under pressure.[60] CsF adopts the CsCl structure ($Pm\bar{3}m$), in which a Cs atom is coordinated to 8 F atoms, at pressures higher than 5 GPa (part **Aa**). The coordination number of Cs dramatically decreases while its 5*p* core electrons are forced to participate in bond formation. CsF_2 (C2/m at 20 GPa) consists of linear CsF_2 molecules (part **Ab**). CsF_3 (C2/m) consists of F^- anions and CsF_2^- linear molecular cations at 100 GPa (part **Ac**). When this structure is relaxed to lower pressures (< 30 GPa), the actual formula becomes $Cs^+[F_3]^-$ (part **Ad**). CsF_5 (Fdd2) consists of planar pentagonal (star-fish) CsF_5 molecules at 150 GPa (part **Ae**). **B|** Structures of HgF_n compounds under pressure (Ref.[70]), including HgF_3 in an $Fm\bar{3}m$ structure at 100 GPa (part **Ba**) and HgF_4 in an I4/m structure at 50 GPa (part **Bb**). HgF_3 adopts the Li_3Bi structure, in which $Hg–F^I$ occupies the tetrahedral sites of the face-centered cubic Hg lattice and $Hg–F^{II}$ occupies the octahedral sites. In contrast, the HgF_4 structure consists of square planar HgF_4 molecules. The coordination number of Hg decreases from that of 14 (8 with F^I + 6 with F^{II}) in HgF_3 to 4 in HgF_4. **C|** Structures of Li_nCs compounds under pressure,[71] including LiCs in the $Pm\bar{3}m$ structure (part **Ca**), Li_2Cs in the I4/mmm structure (part **Cb**), Li_3Cs in the Pnna structure together with the deformed icosahedron containing Li-Li dimers (part **Cc**), Li_4Cs in a C2/m structure together with the tri-capped cube Li polyhedron (part **Cd**), and Li_5Cs in a P2/m structure (part **Ce**). The coordination number of Cs increases from 8 in LiCs to 10 in Li_2Cs, to 12 in Li_3Cs and then decreases to 11 in Li_4Cs and Li_5Cs. MgXe and Mg_2Xe adopt the same structures as LiCs and Li_2Cs, respectively. Parts **Ab – Ae** are adapted from REF [60]. Springer Nature Limited, parts **Ba – Bb** are adapted with permission from REF [70]. Willey-VCH, parts **Ca – Ce** are adapted from REF [71]. Springer Nature Limited.

`

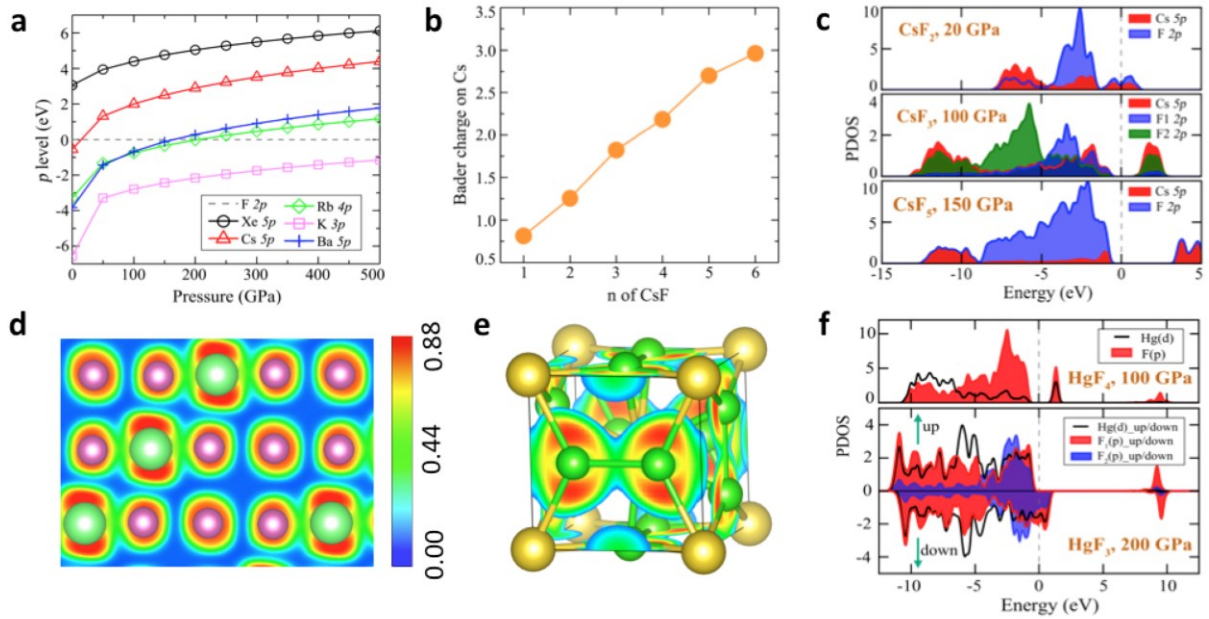

Figure 3. Chemistry of core electrons. Electronic structures and bonding features of compounds formed because of the activation of core electrons under pressure. **a** | Energies of the outermost filled *p* levels of select elements, including F, Xe, Cs, Rb, K and Ba, as a function of external pressure[60]. The density functional theory (DFT) calculations show that the Cs 5*p* energy becomes higher than the F 2*p* energy at pressures higher than 10 GPa, indicating that Cs can be oxidized by F above the +I state under these conditions. **b** | Calculated charges of Cs in CsF_n at 100 GPa, using Bader's quantum theory of atoms in molecules (QTAIM) analysis.[247] The Bader charges increase almost linearly with increasing F composition and are seemingly larger than +1, strongly indicating the involvement of Cs 5*p* electrons in forming bonds with F (Ref.[60]). **c** | Calculated projected density of states (PDOS) for CsF_n (n=2,3,5) at 20, 100, and 150 GPa, respectively. The results show strong overlap of the Cs 5*p* and F 2*p* states below and above the Fermi level, indicating the involvement of Cs 5*p* electrons in the formation of covalent bonds with F (Ref.[60]). **d** | Calculated electron localization function (ELF) for CsF_3 at 100 GPa. The large ELF values in the regions between Cs and F reveal strong covalent bonds between them [60]. **e** | ELF for $NaCl_3$ at 100 GPa (Ref. [50]). The results show that the bonding feature of $NaCl_3$ is completely different to that of CsF_n compounds. There is no evidence of new Na–Cl bonds that involve Na core electrons. Instead, Cl atoms form homonuclear bonds under pressure. **f** | Calculated PDOS for HgF_4 at 100 GPa and HgF_3 at 200 GPa (Ref.[70]). The results show that Hg 5*d* electrons are involved in the formation of Hg–F bonds because these states overlap with the F 2*p* states below and above the Fermi level. Hg in HgF_4 is in a d^8 configuration, which gives rise to a small gap owing to the split of *d* levels in the square planar crystal field. In contrast, Hg in HgF_3 is in a d^9 configuration, leading to a metallic state. HgF_3 is predicted to be metallic and ferromagnetic, and exhibits an electronic structure that resembles a transparent hole conductor. Parts **a – d** are adapted from REF [60]. Springer Nature Limited. Part **f** is adapted with permission from REF [70]. Willey-VCH

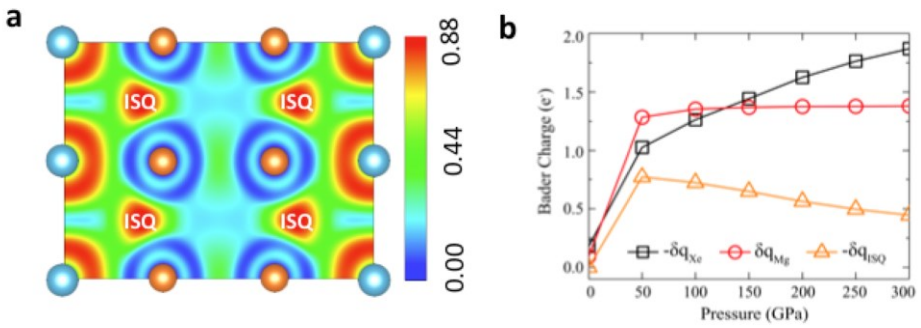

Figure 4 | Chemistry of non-valence orbitals. Mg_2Xe is an example of a compound whose formation involves non-valence Xe 5*d* orbitals[192] . **a |** Calculated electron localization function (ELF) for Mg_2Xe at 200 GPa in the I4/mmm structure showing a cut of the (100) plane. Large ELF values not only appear at the Xe and Mg sites, but also at the interstitial sites, indicating that Mg_2Xe is a high-pressure electride (HPE). Compared to Mg, which becomes an HPE at about 800 GPa[196] , the presence of Xe atoms increases the interstitial volume, thereby greatly lowering the pressure for forming an HPE. **b |** The Bader charges of Xe, Mg and interstitial quasi-atoms (ISQs) in Mg_2Xe as a function of pressure. The plot shows a large charge transfer from Mg to Xe, indicating that Xe is reduced in this unusual compound. Mg_2Xe is an HPE at a pressure as low as 50 GPa. At higher pressures, the ISQ transfers charge to Xe because the Xe 5*d* orbital energies decrease relative to that of the ISQ orbital. Both parts **a** and **b** are adapted with permission from REF [192]. American Chemical Society.

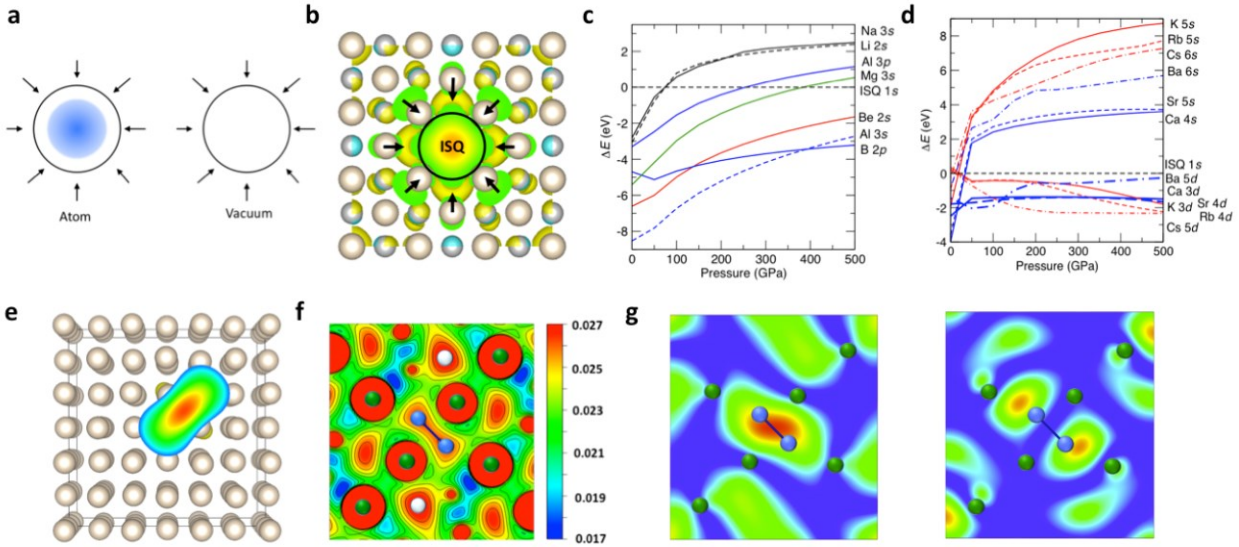

Figure 5. Quasiatoms and their chemistry. Quantum orbitals of an interstitial quasi-atom (ISQ) and their behavior, as calculated using first principles, under pressure[68,229,230]. **a |** Schematics of compressing an atom versus compressing an ISQ. The blue region represents the core that repels the valence electrons. **b|** Helium matrix model that is used to examine the orbital

energies of atomic and ISQ orbitals as a function of pressure. The isosurface (iso = 0.001 $e \cdot bohr^{-3}$) shows the 1*s* orbital of ISQ. **c |** Orbital energies (in the helium containment model) of an electron in the highest occupied orbital of selected group 1, 2, and 13 elements, referenced to the energy of an electron in the 1s orbital of an ISQ as a function of pressure. **d |** Energies of the valence *s* orbitals and the unoccupied *d* orbitals of several alkali metals referenced to an ISQ 1*s* orbital under pressure. The valence orbitals of atoms are lower in energy than the 1*s* orbital of an ISQ at ambient conditions. However, because of the presence of the core region, the energies of most valence orbitals (such as *s* and *p*) increase faster than that of the ISQ under pressure and might surpass the latter at large enough pressures. In contrast, the energies of d orbitals decrease relative to that of the ISQ. Therefore, the presence of unoccupied *d* orbitals might prevent the formation of HPEs. **e |** Covalent bonds can occur between quasi-atoms as can be observed from the charge density of the bonding state between two ISQs located on the neighboring sites of a He fcc matrix model.[229] **f |** Charge density of HPE Li at 60 GPa. The plot shows the total valence charge density ($e \cdot bohr^{-3}$) in a plane perpendicular to the b–c plane, Miller index (011). **g |** Electron densities computed for the bonding (left) and the anti-bonding states (right) of the E^I–E^I pairs in Aba2 Li at the Γ point at 60 GPa. These results show that if the two quasi-atoms are close enough they might form strong covalent bonds. The formation of the ISQ–ISQ bonds and the corresponding split of the energies between bonding and anti-bonding states are the origin of the small band gap in HPE Li under high pressure. Parts a – d are adapted with permission from REF [68]. American Chemical Society, parts f – g are adapted with permission from REF [230]. Willey-VCH.

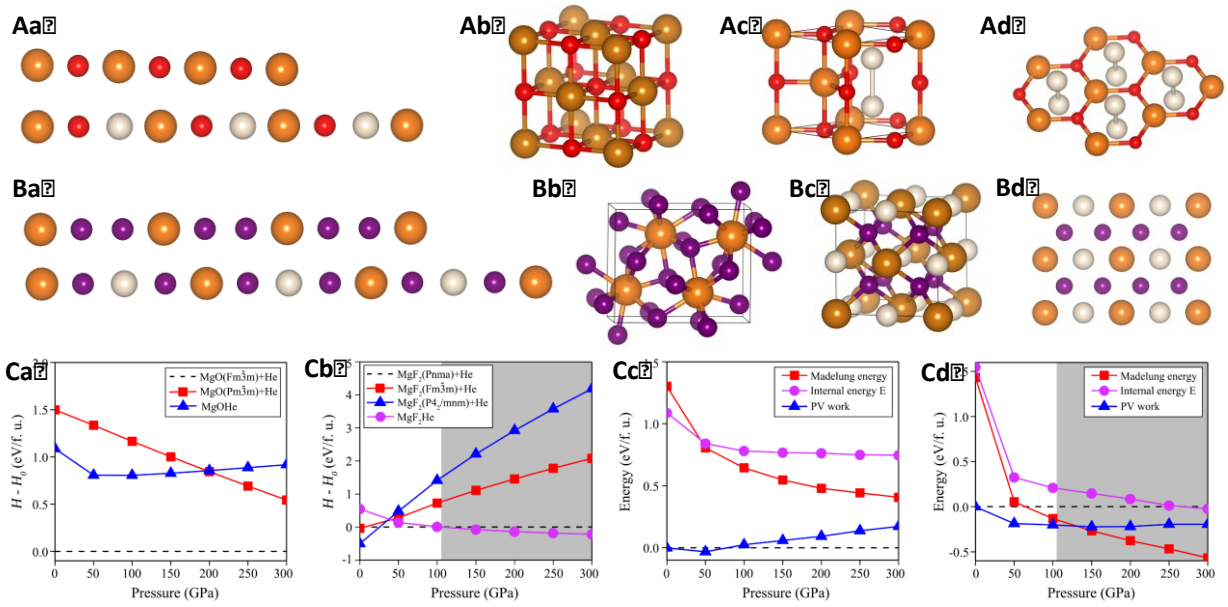

Figure 6. Chemistry without chemical bonds and the mechanism of He insertion in ionic compounds. A | Helium insertion in AB type ionic compounds.[235] The orange, red and white balls represent Mg, O and He atoms. **Aa** | The insertion of He will increase the distances between Mg and O atoms, causing the increase of electrostatic Madelung energy. **Ab** | MgO in the NaCl structure. The arrangement of Mg and O ions resemble that of the AB chain in part Aa. **Ac** | MgOHe in the $P6_3/mmc$ structure. **Ad** | He atoms in MgOHe are located out of the plane to avoid a direct insertion in between Mg and O atoms as shown in Aa. **B** | Helium insertion in AB_2 type ionic compounds.[235] The orange, dark blue and white balls represent Mg, F and He atoms. **Ba** | Insertion of He in between two neighboring F ions alleviates the strong repulsion between the two, therefore lowering the Madelung energy. **Bb** | MgF_2 in the low-symmetry Pnma structure that avoids the close contact of F atoms like the AB_2 chain in part Ba. **Bc** | He inserted MgF_2 structure ($Fm\bar{3}m$). **Bd** | (110) cut plane of MgF_2He in the $Fm\bar{3}m$ structure. The arrangement of Mg, F and He resemble the AB_2He chain in part Ba. **C** | Stability of the He inserted compounds and the change of Madelung energy.[235] **Ca** | The enthalpy difference between MgO+He and MgOHe. **Cb** | The enthalpy difference between MgF_2+He and MgF_2He. **Cc** | Relative changes in PV work, internal energy, E, and Madelung energy for He insertion into MgO. **Cd** | Relative changes in PV work, internal energy E and Madelung energy for He insertion into MgF_2. The areas shaded in gray in **Cb** and **Cd** denote pressures in which the He-inserted compounds is stable. Parts Ca–Cd are adapted from REF [235]. Springer Nature Limited.

Box 1. The basics of a priori crystal structure prediction techniques

The structure of a crystal, the unit cell of which contains N atoms, can be described by $3N+3$ variables (3 unit cell vectors, 3 cell angles, and $3N-3$ atomic coordinates). Because the shape of the potential energy surface (PES) is unknown, locating the global minimum requires comparing the free energies of all of the local minima. However, because the number of minima increases exponentially with N (Ref.[248]), this brute force approach can only be used to study simple systems. A number of well-known metaheuristics designed to solve optimization problems have been adapted towards crystal structure prediction (CSP). None of these algorithms are guaranteed to find the optimal solution, but the chances of success can be dramatically enhanced by focusing the search on chemically sensible structures (for example, those with reasonable interatomic distances, atomic orderings and cell volumes). Because the stoichiometries and crystal structures of high-pressure phases can differ drastically from those known at 1 atm (Refs[20,249]), the algorithms used to predict them cannot benefit from information found in materials databases and require first-principles approaches, such as density functional theory, to optimize the structures and evaluate their stability. Currently, these algorithms can reliably predict the global minimum of elemental or binary systems the unit cells of which contain < 50 atoms, and advances towards more complex systems are being made [6,21,250,69,251–253].

Random structure search. This is a straightforward and yet still very powerful CSP method, in which all of the $3N+3$ degrees of freedom of a crystal are chosen randomly, but sensibly. The ab initio random structure searching (AIRSS)[12,13] method is the best known algorithm of this type.

Evolutionary/genetic algorithms (EA/GA). These algorithms employ concepts from evolutionary biology to sample the PES. First, they generate a chemically sensible, random set of structures (seeding with particular structures is also possible), which are locally optimized. The energy or enthalpy of each structure is used to determine its fitness, or probability to be chosen as a parent for a subsequent generation. Children structures are constructed by cutting and splicing two parental structures, or by mutating a single parent (for example, by permuting atoms of different types, changing the shape of the unit cell or by displacing atoms). EAs can sample the whole PES, and they learn from their history. USPEX[16,18] and XtalOpt[254,255] are among the most widely used EAs for high pressure systems.

Particle swarm optimization (PSO). This approach, implemented in the CALYPSO code[22,24], was inspired by the collective movement of large groups of animals. (Quasi)random structures are generated, and the trajectory used to sample the PES is determined by a structure's position and velocity, as well as the position of the global minimum. The PES can be explored globally or locally and random structures are continuously injected into the search to ensure that the whole PES is sampled.

Minima hopping. This method uses molecular dynamics (MD) to explore the PES locally[256,257]. Each structure, which is optimized to the nearest minimum, is accepted or rejected based on its energy relative to that of its predecessor. The energy difference corresponding to an allowed move and the kinetic energy of the MD simulations are constantly altered so that 50% of the structures are accepted. If a minimum is re-visited, the kinetic energy is increased so new regions of the PES can be explored.

Metadynamics. This technique employs a history-dependent bias potential to accelerate sampling of the PES by overcoming barriers so that new minima can be discovered[258]. It may be used to search the PES locally or to study reaction pathways and rare phenomena.

Simulated annealing. Here the PES is explored using the Metropolis Monte Carlo method[259,260]. The temperature of the simulation is gradually decreased during a run so that fewer high-energy structures are accepted, thereby mimicking the physical annealing process.

Box 2. Rules that describe structure and bonding changes under pressure

Because many factors are important in determining the structure that a solid adopts, codifying them in a set of rules is a difficult task. Pauling's five rules of ionic crystal structures at ambient pressure come closest[62]:

1. The sum of the ionic radii determines the cation-anion distance, and the cation/anion radius ratio determines the coordination number;
2. A stable ionic structure is arranged to preserve local electroneutrality, so that the sum of the strengths of the electrostatic bonds to an anion equals the charge on that anion;
3. The sharing of edges and particular faces by two anionic polyhedra decreases the stability of an ionic structure;
4. In a crystal containing different cations, those of high valency and small coordination number tend not to share polyhedron elements with one another;
5. The number of essentially different kinds of constituents in a crystal tends to be small.

The way in which the structures of solids, and their bonding evolve under pressure adhere to a few trends, many of which have been summarized in several sets of rules, including those of Prewitt and Downs;[63] Grochala, Hoffmann, Feng, and Ashcroft;[64] Zhang, Wang, Lv and Ma [6]. A number of the emergent trends agree with our chemical intuition. For example, under high pressure the structures of solid compounds tend to:

i. become more homogeneous by compressing the longer and weaker bonds the most [6,63,64];
ii. assume close-packed structures[6,63];
iii. increase coordination numbers[63,64];
iv. have higher symmetry [64] ;
v. exhibit more delocalized electronic states, which eventually bring about insulator-to-metal transitions [6,64]

However, phenomena that cannot be intuitively understood have been observed especially in recent studies of atypical compounds. For example, it has been proposed that deviation from close-packing of spheres may be used to achieve higher density [64], electrons might detach from atoms [6,64], and repopulation of the atomic orbitals might change the chemical identity of the atoms [6,64].

BOX3. Several fundamental concepts for chemistry under pressure

The key factors that lead to the formation of atypical compounds and/or new chemical properties under high pressure can be summarized as:

i. Pressure enhances the formation of homonuclear bonds.
ii. Pressure changes/reorders the energies of quantum mechanical states (whether they be atom centered or not), resulting in the redistribution of electron density, which thereby changes an element's chemistry.
iii. Increased electrostatic interactions induce large driving forces for some reactions that involve ions and polar molecules.

To further understand the way in which chemical bonds are perturbed under pressure, we can use a diatomic Hückel model.[72] For diatomic molecules, the Hückel secular equation and the corresponding determinant are:

$$\begin{pmatrix} \alpha_A & \beta \\ \beta & \alpha_B \end{pmatrix} \begin{pmatrix} c_1 \\ c_2 \end{pmatrix} = E \begin{pmatrix} c_1 \\ c_2 \end{pmatrix} \begin{vmatrix} \alpha_A - E & \beta \\ \beta & \alpha_B - E \end{vmatrix} = 0$$

in which, $\alpha_{A,B} = \langle \varphi_{A,B} | H | \varphi_{A,B} \rangle$ are the Coulomb integrals, and $\beta = \langle \varphi_A | H | \varphi_B \rangle$ is the resonance integral. The overlap integrals are neglected in the Hückel model. By solving the secular equation, one can find the energies of the bonding and the antibonding states as the eigenvalues E_1 and E_2. The bond energy can be expressed as:

$$E_b = E_2 - E_1 = \sqrt{(\alpha_A - \alpha_B)^2 + 4\beta^2}$$

Under increasing compression, all Hamiltonian integrals change. Whereas $\alpha_A - \alpha_B$ might either increase or decrease depending on the nature of the valence orbitals of atoms A and B, β always increases under compression. Therefore, let us consider the change of β and assume $\alpha_A - \alpha_B$ remains unchanged. As β increases by an amount $\delta\beta$, the change in E_b is:

$$\delta E_b = \frac{\partial E_b}{\partial \beta} \delta\beta = \frac{4\beta}{\sqrt{(\alpha_A - \alpha_B)^2 + 4\beta^2}} \delta\beta$$

On one extreme, we have homonuclear bonds (panel on the left), for which $\alpha_A = \alpha_B$, therefore $\delta E_b = 2\delta\beta$. In the opposite case, we have strongly polar heteronuclear bonds (panel on the right) for which $\alpha_A \gg \alpha_B$ (assuming A is the electron donor), therefore $\alpha_A - \alpha_B \gg 2\beta$ and δE_b can be simplified as:

$$\delta E_b \approx \frac{4\beta}{\alpha_A - \alpha_B} \delta\beta \ll 2\delta\beta$$

These results show that while bond energies increase, and the bonds therefore become stronger under compression, this effect is more significant for less-polar bonds. ***Hence, pressure can increase the stability of homonuclear bonds or those that are less polar relative to highly polar bonds or ionic bonds.***

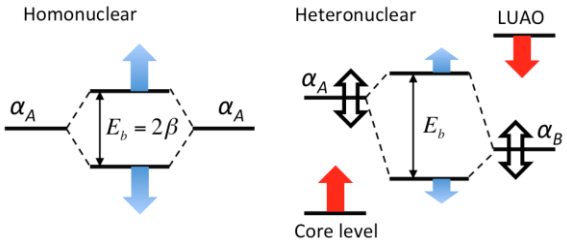

The arrows in the schematic represent the response of the chemical bonding states and the atomic orbitals to the increasing pressure. Blue arrows correspond to the relative energetic shifts of bonding and antibonding states of diatomic bonds, which are larger for homonuclear bonds than for heteronuclear bond. Black arrows indicate the relative shifts of valence orbital energies of atoms A and B; they can be in both directions. Red arrows correspond to the relative shifts of the core levels and the lowest unoccupied atomic orbitals (LUAO). The chemical behavior of the atoms might change if the core level become close to or above α_B or the LUAO levels become close to or below α_A.

References

1. McMillan, P. F. Pressing on: the legacy of Percy W. Bridgman. *Nat. Mater.* **4**, 715–718 (2005).
2. Hemley, R. J. Percy W. Bridgman's second century. *High Pressure Research* **30**, 581–619 (2010).
3. Dubrovinsky, L., Dubrovinskaia, N., Prakapenka, V. B. & Abakumov, A. M. Implementation of micro-ball nanodiamond anvils for high-pressure studies above 6 Mbar. *Nat. commun.* **3**, 1163 (2012).
4. Dubrovinsky, L. *et al.* The most incompressible metal osmium at static pressures above 750 gigapascals. *Nature* **525**, 226–229 (2015).
5. Dubrovinskaia, N. *et al.* Terapascal static pressure generation with ultrahigh yield strength nanodiamond. *Sci. Adv.* **2**, e1600341 (2016).
6. Zhang, L., Wang, Y., Lv, J. & Ma, Y. Materials discovery at high pressures. *Nature Reviews Materials* **2**, 17005 (2017).
7. Brazhkin, V. V. High-pressure synthesized materials: Treasures and hints. *High Pressure Research* **27**, 333–351 (2007).
8. Shen, G. & Mao, H. K. High-pressure studies with x-rays using diamond anvil cells. *Rep. Prog. Phys.* **80**, 016101 (2017).
9. Badding, J. V. High-pressure synthesis, characterization, and tuning of solid state materials. *Annu. Rev. Mater. Sci.* **28**, 631–658 (1998).
10. Mao, H. K., Chen, X. J., Ding, Y., Li, B. & Wang, L. Solids, liquids, and gases under high pressure. *Rev. Mod. Phys.* **90**, 015007 (2018).
11. Pickard, C. J. & Needs, R. J. High-pressure phases of silane. *Phys. Rev. Lett.* **97**, 045504 (2006).
12. Pickard, C. J. & Needs, R. J. Structures at high pressure from random searching. *Phys. Status Solidi B* **246**, 536–540 (2009).
13. Pickard, C. J. & Needs, R. J. Ab initio random structure searching. *J. Phys.: Condens. Matter* **23**, 053201 (2011).
14. Needs, R. J. & Pickard, C. J. Perspective: Role of structure prediction in materials discovery and design. *Apl Materials* **4**, 053210 (2016).
15. Oganov, A. R. & Glass, C. W. Crystal structure prediction using ab initio evolutionary techniques: Principles and applications. *J. Chem. Phys.* **124**, 244704 (2006).
16. Glass, C. W., Oganov, A. R. & Hansen, N. USPEX - Evolutionary crystal structure prediction. *Comput. Phys. Commun.* **175**, 713–720 (2006).
17. Oganov, A. R., Lyakhov, A. O. & Valle, M. How evolutionary crystal structure prediction works and why. *Acc. Chem. Res.* **44**, 227–237 (2011).
18. Lyakhov, A. O., Oganov, A. R., Stokes, H. T. & Zhu, Q. New developments in evolutionary structure prediction algorithm USPEX. *Comput. Phys. Commun.* **184**, 1172–1182 (2013).
19. Zhu, Q., Oganov, A. R. & Zhou, X. F. Crystal structure prediction and its application in earth and materials sciences. *Top. Curr. Chem.* **345**, 223–256 (2014).
20. Zurek, E. & Grochala, W. Predicting crystal structures and properties of matter under extreme conditions via quantum mechanics: The pressure is on. *Phys. Chem. Chem. Phys.* **17**, 2917–2934 (2015).

21. Zurek, E. Discovering new materials via a priori crystal structure prediction. *Reviews in Computational Chemistry* 274–326 (2016).
22. Wang, Y., Lv, J., Zhu, L. & Ma, Y. Crystal structure prediction via particle-swarm optimization. *Phys. Rev. B* **82**, 094116 (2010).
23. Wang, Y., Lv, J., Zhu, L. & Ma, Y. CALYPSO: A method for crystal structure prediction. *Comput. Phys. Commun.* **183**, 2063–2070 (2012).
24. Wang, H. *et al.* CALYPSO structure prediction method and its wide application. *Comput. Mater. Sci.* **112**, 406–415 (2016).
25. Su, C. *et al.* Construction of crystal structure prototype database: Methods and applications. *J. Phys.: Condens. Matter* **29**, 165901 (2017).
26. McMahon, M. I. & Nelmes, R. J. High-pressure structures and phase transformations in elemental metals. *Chem. Soc. Rev.* **35**, 943–963 (2006).
27. Hemley, R. J., Jephcoat, A. P., Mao, H. K., Ming, L. C. & Manghnani, M. H. Pressure-induced amorphization of crystalline silica. *Nature* **334**, 52–54 (1988).
28. Itie, J. P. *et al.* Pressure-induced coordination changes in crystalline and vitreous GeO_2. *Phys. Rev. Lett.* **63**, 398–401 (1989).
29. Nunez-Regueiro, M., Marques, L., Hodeau, J. L., Bethoux, O. & Perroux, M. Polymerized fullerite structures. *Phys. Rev. Lett.* **74**, 278–281 (1995).
30. Blank, V. D. *et al.* High-pressure polymerized phases of C_{60}. *Carbon* **36**, 319–343 (1998).
31. Iota, V. Quartzlike carbon dioxide: An optically nonlinear extended solid at high pressures and temperatures. *Science* **283**, 1510–1513 (1999).
32. Yong, X. *et al.* Crystal structures and dynamical properties of dense CO_2. *PNAS* **113**, 11110 (2016).
33. Yoo, C. S. *et al.* Crystal structure of carbon dioxide at high pressure: "Superhard" polymeric carbon dioxide. *Phys. Rev. Lett.* **83**, 5527–5530 (1999).
34. Lin, J. F. & Tsuchiya, T. Spin transition of iron in the earth's lower mantle. *Physics of the Earth and Planetary Interiors* **170**, 248–259 (2008).
35. Lyubutin, I. S. *et al.* Spin transition of Fe^{2+} in ringwoodite $(Mg, Fe)_2SiO_4$ at high pressures. *Am. Mineral.* **98**, 1803–1810 (2013).
36. Lin, J.-F. *et al.* Pressure-induced electronic spin transition of iron in magnesiowustite-(Mg, Fe)O. *Phys. Rev. B* **73**, 113107 (2006).
37. Drickamer, H. G. & Frank, C. W. Electronic transitions and the high pressure chemistry and physics of solids. (Springer Science & Business Media, 2013).
38. Buzea, C. & Robbie, K. Assembling the puzzle of superconducting elements: A review. *Supercond. Sci. Technol.* **18**, 1–8 (2005).
39. Schilling, J. S. Superconductivity in the alkali metals. *High Pressure Research* **26**, 145–163 (2006).
40. Sakata, M., Nakamoto, Y., Shimizu, K., Matsuoka, T. & Ohishi, Y. Superconducting state of Ca-VII below a critical temperature of 29 K at a pressure of 216 GPa. *Phys. Rev. B* **83**, 220512 (2011).
41. Matsuoka, T. *et al.* Pressure-induced superconductivity in $CaLi_2$. *Phys. Rev. Lett.* **100**, 197003 (2008).
42. Chen, X. J. *et al.* Superconducting behavior in compressed solid SiH_4 with a layered structure. *Phys. Rev. Lett.* **101**, 077002 (2008).
43. Li, Y., Hao, J., Liu, H., Li, Y. & Ma, Y. The metallization and superconductivity of dense hydrogen sulfide. *J. Chem. Phys.* **140**, 174712 (2014).

44. Duan, D. *et al.* Pressure-induced metallization of dense $(H_2S)_2H_2$ with high-T_c superconductivity. *Scientific reports* **4**, 6968 (2014).
45. Drozdov, A. P., Eremets, M. I., Troyan, I. A., Ksenofontov, V. & Shylin, S. I. Conventional superconductivity at 203 kelvin at high pressures in the sulfur hydride system. *Nature* **525**, 73–76 (2015).
46. Errea, I. *et al.* High-pressure hydrogen sulfide from first principles: a strongly anharmonic phonon-mediated superconductor. *Phys. Rev. Lett.* **114**, 157004 (2015).
47. Akashi, R., Sano, W., Arita, R. & Tsuneyuki, S. Possible 'Magneli' phases and self-alloying in the superconducting sulfur hydride. *Phys. Rev. Lett.* **117**, 075503 (2016).
48. Li, X., Liu, H. & Peng, F. Crystal structures and superconductivity of technetium hydrides under pressure. *Phys. Chem. Chem. Phys.* **18**, 28791–28796 (2016).
49. Errea, I. *et al.* Quantum hydrogen-bond symmetrization in the superconducting hydrogen sulfide system. *Nature* **532**, 81–84 (2016).
50. Zhang, W. W. *et al.* Unexpected stable stoichiometries of sodium chlorides. *Science* **342**, 1502–1505 (2013).
51. Peng, F., Yao, Y., Liu, H. & Ma, Y. Crystalline LiN_5 predicted from first-principles as a possible high-energy material. *J. Phys. Chem. Lett.* **6**, 2363–2366 (2015).
52. Shen, Y. *et al.* Novel lithium-nitrogen compounds at ambient and high pressures. *Scientific reports* **5**, 14204 (2015).
53. Hemley, R. J., Ahart, M., Liu, H. & Somayazulu, M. Superconductivity and pressure: On the road to room-temperature superconductivity. in *Proceedings of the International Symposium - Superconductivity and Pressure: A Fruitful Relationship on the Road to Room Temperature Superconductivity* (ed. Alario y Franco, M. A.) 199–213 (2019).
54. Liu, H., Naumov, I. I., Hoffmann, R., Ashcroft, N. W. & Hemley, R. J. Potential high-T_c superconducting lanthanum and yttrium hydrides at high pressure. *PNAS* **114**, 6990 (2017).
55. Somayazulu, M. *et al.* Evidence for superconductivity above 260 K in lanthanum superhydride at megabar pressures. *Phys. Rev. Lett.* **122**, 027001 (2019).
56. Peng, F. *et al.* Hydrogen clathrate structures in rare earth hydrides at high pressures: Possible route to room-temperature superconductivity. *Phys. Rev. Lett.* **119**, 107001 (2017).
57. Drozdov, A. P. *et al.* Superconductivity at 250 K in lanthanum hydride under high pressures. *Nature* **569**, 528–531 (2019).
58. Geballe, Z. M. *et al.* Synthesis and stability of lanthanum superhydrides. *Angew. Chem. Int. Ed. Engl.* **57**, 688–692 (2018).
59. Zhu, L., Liu, H., Pickard, C. J., Zou, G. & Ma, Y. Reactions of xenon with iron and nickel are predicted in the earth's inner core. *Nat. Chem.* **6**, 644–648 (2014).
60. Miao, M. S. Cesium in high oxidation states and as a *p*-block element. *Nat. Chem.* **5**, 846–852 (2013).
61. Dong, X. *et al.* A stable compound of helium and sodium at high pressure. *Nat. Chem.* **9**, 440–445 (2017).
62. Pauling, L. The nature of the chemical bond and the structure of molecules and crystals: An introduction to mode. (Cornell University Press, 1960).
63. Prewitt, C. T. & Downs, R. T. Chapter 9 High-pressure crystal chemistry.
64. Grochala, W., Hoffmann, R., Feng, J. & Ashcroft, N. W. The chemical imagination at work in very tight places. *Angew. Chem. Int. Ed. Engl.* **46**, 3620–3642 (2007).
65. Ashcroft, N. W. & Mermin, N. D. *Solid State Physics*. (Holt, Rinehart and Winston, 1976).

66. Hanfland, M., Syassen, K., Christensen, N. E. & Novikov, D. L. New high-pressure phases of lithium. *Nature* **408**, 174–178 (2000).
67. Ma, Y. *et al.* Transparent dense sodium. *Nature* **458**, 182–185 (2009).
68. Miao, M.-S. & Hoffmann, R. High pressure electrides: A predictive chemical and physical theory. *Acc. Chem. Res.* **47**, 1311–1317 (2014).
69. Oganov, A. R., Pickard, C. J., Zhu, Q. & Needs, R. J. Structure prediction drives materials discovery. *Nature Reviews Materials* **4**, 331–348 (2019).
70. Botana, J. *et al.* Mercury under pressure acts as a transition metal: Calculated from first principles. *Angew. Chem. Int. Ed. Engl.* **54**, 9280–9283 (2015).
71. Botana, J. & Miao, M. S. Pressure-stabilized lithium caesides with caesium anions beyond the -1 state. *Nat. commun.* **5**, 4861 (2014).
72. Housecroft, C. E. & Sharpe, A. G. Inorg. chem. (Pearson, 2012).
73. Cotton. Advanced inorganic chemistry, 6th ED. (Wiley India Pvt. Limited, 2007).
74. Janka, O. & Kauzlarich, S. M. Zintl compounds. *Encyclopedia of Inorganic and Bioinorganic Chemistry* 1–14 (2014).
75. Scharfe, S., Kraus, F., Stegmaier, S., Schier, A. & Fässler, T. F. Zintl ions, cage compounds, and intermetalloid clusters of group 14 and group 15 elements. *Angew. Chem. Int. Ed.* **50**, 3630–3670 (2011).
76. Peng, F., Miao, M., Wang, H., Li, Q. & Ma, Y. Predicted lithium-boron compounds under high pressure. *J. Am. Chem. Soc.* **134**, 18599–18605 (2012).
77. Hermann, A. *et al.* LiB and its boron-deficient variants under pressure. *Phys. Rev. B* **86**, 144110 (2012).
78. Ashcroft, N. W. Hydrogen dominant metallic alloys: High temperature superconductors? *Phys. Rev. Lett.* **92**, 187002 (2004).
79. Ashcroft, N. W. Metallic hydrogen - a high-temperature superconductor. *Phys. Rev. Lett.* **21**, 1748 (1968).
80. Struzhkin, V. V. *et al.* Synthesis of sodium polyhydrides at high pressures. *Nat. Commun.* **7**, 1–8 (2016).
81. Pépin, C., Loubeyre, P., Occelli, F. & Dumas, P. Synthesis of lithium polyhydrides above 130 GPa at 300 K. *PNAS* **112**, 7673–7676 (2015).
82. Mishra, A. K. *et al.* New calcium hydrides with mixed atomic and molecular hydrogen. *J. Phys. Chem. C* **122**, 19370–19378 (2018).
83. Hooper, J. & Zurek, E. Rubidium polyhydrides under pressure: Emergence of the linear H_3^- species. *Chemistry* **18**, 5013–5021 (2012).
84. Shamp, A., Hooper, J. & Zurek, E. Compressed cesium polyhydrides: Cs^+ sublattices and H_3^- three-connected nets. *Inorg. Chem.* **51**, 9333–9342 (2012).
85. Wang, H., Li, X., Gao, G., Li, Y. & Ma, Y. Hydrogen-rich superconductors at high pressures. *Wiley Interdisciplinary Reviews: Computational Molecular Science* **8**, e1330 (2018).
86. Wang, Z., Wang, H., Tse, J. S., Iitaka, T. & Ma, Y. Stabilization of H_3^+ in the high pressure crystalline structure of H_nCl (n = 2–7). *Chem. Sci.* **6**, 522–526 (2014).
87. Hooper, J., Terpstra, T., Shamp, A. & Zurek, E. Composition and constitution of compressed strontium polyhydrides. *J. Phys. Chem. C* **118**, 6433–6447 (2014).
88. Wang, Y., Wang, H., Tse, J. S., Iitaka, T. & Ma, Y. Structural morphologies of high-pressure polymorphs of strontium hydrides. *Phys. Chem. Chem. Phys.* **17**, 19379–19385 (2015).

89. Wang, H., Tse, J. S., Tanaka, K., Iitaka, T. & Ma, Y. Superconductive sodalite-like clathrate calcium hydride at high pressures. *PNAS* **109**, 6463 (2012).
90. Shamp, A. & Zurek, E. Superconductivity in hydrides doped with main group elements under pressure. *Novel Superconducting Materials* **3**, 14–22 (2017).
91. Martinez-Canales, M. *et al.* Novel structures and superconductivity of silane under pressure. *Phys. Rev. Lett.* **102**, 087005 (2009).
92. Cui, W. *et al.* Hydrogen segregation and its roles in structural stability and metallization: silane under pressure. *Scientific reports* **5**, 13039 (2015).
93. Li, Y. *et al.* Superconductivity at approximately 100 K in dense $SiH_4(H_2)_2$ predicted by first principles. *PNAS* **107**, 15708–15711 (2010).
94. Mahdi Davari Esfahani, M. *et al.* Superconductivity of novel tin hydrides (Sn_nH_m) under pressure. *Scientific reports* **6**, 22873 (2016).
95. Gao, G. *et al.* Superconducting high pressure phase of germane. *Phys. Rev. Lett.* **101**, 107002 (2008).
96. Yuan, Y. *et al.* Stoichiometric evolutions of PH_3 under high pressure: Implication for high-T_c superconducting hydrides. *National Science Review* **6**, 524–531 (2019).
97. Flores-Livas, J. A., Sanna, A. & Gross, E. K. U. High temperature superconductivity in sulfur and selenium hydrides at high pressure. *Eur. Phys. J. B* **89**, 1–6 (2016).
98. Flores-Livas, J. A. *et al.* Superconductivity in metastable phases of phosphorus-hydride compounds under high pressure. *Phys. Rev. B* **93**, 020508 (2016).
99. Errea, I. *et al.* Quantum crystal structure in the 250-kelvin superconducting lanthanum hydride. *Nature* **578**, 66–69 (2020).
100. Zurek, E. & Bi, T. High-temperature superconductivity in alkaline and rare earth polyhydrides at high pressure: A theoretical perspective. *J. Chem. Phys.* **150**, 050901 (2019).
101. Li, P. *et al.* New high pressure phase of yttrium metal under ultrahigh pressure. *Comput. Mater. Sci.* **159**, 428–431 (2019).
102. Zurek, E. Viewpoint: Pushing towards room-temperature superconductivity. *Physics* **12**, 1 (2019).
103. Flores-Livas, J. A. *et al.* A perspective on conventional high-temperature superconductors at high pressure: Methods and materials. *Physics Reports* **856**, 1-78 (2020)
104. Etourneau, J. & Hagenmuller, P. Structure and physical features of the rare-earth borides. *Philosophical Magazine B* **52**, 589–610 (1985).
105. Harran, I., Chen, Y., Wang, H. & Ni, Y. Pressure induced evolution of structures and properties of iron tetraboride. *Crystengcomm* **20**, 3928–3935 (2018).
106. Zhang, X. *et al.* First-principles structural design of superhard material of ZrB_4. *Phys. Chem. Chem. Phys.* **15**, 20894–20899 (2013).
107. Li, X., Tao, Y. & Peng, F. Pressure and temperature induced phase transition in WB_4: A first principles study. *J. Alloys Compd.* **687**, 579–585 (2016).
108. Li, X. & Peng, F. Predicted superhard phases of Zr-B compounds under pressure. *Phys. Chem. Chem. Phys.* **12**, 15609-15614 (2019).
109. Zhang, G., Bai, T., Zhao, Y. & Hu, Y. A new superhard phase and physical properties of ZrB_3 from first-principles calculations. *Materials (Basel)* **9**, 703 (2016).
110. Chu, B. *et al.* Structural, mechanical, and electronic properties of Rh_2B and RhB_2: First-principles calculations. *Scientific reports* **5**, 10500 (2015).

111. Wang, Q. *et al.* Novel high-pressure phase of RhB: First-principles calculations. *J. Phys. Chem. C* **115**, 19910–19915 (2011).
112. Nagamatsu, J., Nakagawa, N., Muranaka, T., Zenitani, Y. & Akimitsu, J. Superconductivity at 39 K in magnesium diboride. *Nature* **410**, 63–64 (2001).
113. Kolmogorov, A. N. *et al.* New superconducting and semiconducting Fe-B compounds predicted with an ab initio evolutionary search. *Phys. Rev. Lett.* **105**, 217003 (2010).
114. Gou, H. *et al.* Discovery of a superhard iron tetraboride superconductor. *Phys. Rev. Lett.* **111**, 157002 (2013).
115. Kolmogorov, A. N. & Curtarolo, S. Theoretical study of metal borides stability. *Phys. Rev. B* **74**, 224507 (2006).
116. Kolmogorov, A. N. & Curtarolo, S. Prediction of different crystal structure phases in metal borides: A lithium monoboride analog to MgB_2. *Phys. Rev. B* **73**, 180501 (2006).
117. Kolmogorov, A. N., Calandra, M. & Curtarolo, S. Thermodynamic stabilities of ternary metal borides: An *ab initio* guide for synthesizing layered superconductors. *Phys. Rev. B* **78**, 094520 (2008).
118. Hermann, A., McSorley, A., Ashcroft, N. W. & Hoffmann, R. From wade–mingos to zintl–klemm at 100 GPa: Binary compounds of boron and lithium. *J. Am. Chem. Soc.* **134**, 18606–18618 (2012).
119. Kolmogorov, A. N., Hajinazar, S., Angyal, C., Kuznetsov, V. L. & Jephcoat, A. P. Synthesis of a predicted layered LiB via cold compression. *Phys. Rev. B* **92**, 144110 (2015).
120. Wang, H., LeBlanc, K. A., Gao, B. & Yao, Y. Thermodynamic ground state of MgB_6 predicted from first principles structure search methods. *J. Chem. Phys.* **140**, 044710 (2014).
121. Benson, D. *et al.* Lithium and calcium carbides with polymeric carbon structures. *Inorg. Chem.* **52**, 6402–6406 (2013).
122. Li, Y. L. *et al.* Pressure-induced superconductivity in CaC_2. *PNAS* **110**, 9289–9294 (2013).
123. Zhong, X. *et al.* Pressure stabilization of long-missing bare C_6 hexagonal rings in binary sesquicarbides. *Chem. Sci.* **5**, 3936–3940 (2014).
124. Feng, C. *et al.* First-principle study of pressure-induced phase transitions and electronic properties of electride Y_2C. *Solid State Commun.* **266**, 34–38 (2017).
125. Guo, Y. *et al.* Pressure-induced structural transformations and polymerization in ThC_2. *Scientific reports* **7**, 45872 (2017).
126. Liu, H., Gao, G., Li, Y., Hao, J. & Tse, J. S. Crystal structures and chemical bonding of magnesium carbide at high pressure. *J. Phys. Chem. C* **119**, 23168–23174 (2015).
127. Liu, H., Naumov & Hemley, R. J. Dense hydrocarbon structures at megabar pressures. *J. Phys. Chem. Lett.* **7**, 4218–4222 (2016).
128. Feng, X. *et al.* Carbon network evolution from dimers to sheets in superconducting ytrrium dicarbide under pressure. *Commun. Chem.* **1**, 85 (2018).
129. Du, H. *et al.* Nonmetallization and band inversion in beryllium dicarbide at high pressure. *Scientific reports* **6**, 26398 (2016).
130. Wang, D., Yan, Y., Zhou, D. & Liu, Y. Evolution of crystal and electronic structures of magnesium dicarbide at high pressure. *Scientific reports* **5**, 17815 (2015).
131. Wei, Q., Zhang, Q., Yan, H. & Zhang, M. Cubic C_3N: A new superhard phase of carbon-rich nitride. *Materials (Basel)* **9**, 840 (2016).
132. Medvedev, S. A. *et al.* Phase stability of lithium azide at pressures up to 60 GPa. *J. Phys.: Condens. Matter* **21**, 195404 (2009).

133. Crowhurst, J. C. *et al.* Synthesis and characterization of the nitrides of platinum and Iridium. *Science* **311**, 1275–1278 (2006).
134. Wang, X. *et al.* Polymerization of nitrogen in lithium azide. *J. Chem. Phys.* **139**, 164710 (2013).
135. Li, J. *et al.* Pressure-induced polymerization of nitrogen in potassium azides. *EPL (Europhysics Letters)* **104**, 16005 (2013).
136. Wang, X., Li, J., Zhu, H., Chen, L. & Lin, H. Polymerization of nitrogen in cesium azide under modest pressure. *J. Chem. Phys.* **141**, 044717 (2014).
137. Bykov, M. *et al.* High-pressure synthesis of ultrain compressible hard rhenium nitride pernitride $Re_2(N_2)(N)_2$ stable at ambient conditions. *Nat. Commun.* **10**, 1–8 (2019).
138. Bykov, M. *et al.* Fe-N system at high pressure reveals a compound featuring polymeric nitrogen chains. *Nat. Commun.* **9**, 1–8 (2018).
139. Laniel, D. *et al.* Synthesis of magnesium-nitrogen salts of polynitrogen anions. *Nat. Commun.* **10**, 1–7 (2019).
140. Yu, S. *et al.* Emergence of novel polynitrogen molecule-like species, covalent chains, and layers in magnesium–nitrogen Mg_xN_y phases under high pressure. *J. Phys. Chem. C* **121**, 11037–11046 (2017).
141. Wei, S. *et al.* Alkaline-earth metal (Mg) polynitrides at high pressure as possible high-energy materials. *Phys. Chem. Chem. Phys.* **19**, 9246–9252 (2017).
142. Chen, Y., Cai, X., Wang, H., Wang, H. & Wang, H. Novel triadius-like N_4 specie of iron nitride compounds under high pressure. *Scientific reports* **8**, 10670 (2018).
143. Vij, A., Pavlovich, J. G., Wilson, W. W., Vij, V. & Christe, K. O. Experimental detection of the pentaazacyclopentadienide (pentazolate) anion, cyclo-N_5^-. *Angew. Chem. Int. Ed.* **41**, 3051–3054 (2002).
144. Steele, B. A. & Oleynik, I. I. Sodium pentazolate: A nitrogen rich high energy density material. *Chemical Physics Letters* **643**, 21–26 (2016).
145. Peng, F., Han, Y., Liu, H. & Yao, Y. Exotic stable cesium polynitrides at high pressure. *Scientific reports* **5**, 16902 (2015).
146. Li, J., Sun, L., Wang, X., Zhu, H. & Miao, M. Simple route to metal cyclo-N_5– salt: High-pressure synthesis of CuN_5. *J. Phys. Chem. C* **122**, 22339–22344 (2018).
147. Laniel, D., Weck, G., Gaiffe, G., Garbarino, G. & Loubeyre, P. High-pressure synthesized lithium pentazolate compound metastable under ambient conditions. *J. Phys. Chem. Lett.* **9**, 1600–1604 (2018).
148. Yi, W. *et al.* Packing high-energy together: Binding the power of pentazolate and high-valence metals with strong bonds. *Materials & Design* **193**, 108820 (2020).
149. Weerasinghe, G. L., Pickard, C. J. & Needs, R. J. Computational searches for iron oxides at high pressures. *J. Phys.: Condens. Matter* **27**, 455501 (2015).
150. Hu, Q. *et al.* FeO_2 and FeOOH under deep lower-mantle conditions and earth's oxygen-hydrogen cycles. *Nature* **534**, 241–244 (2016).
151. Hu, Q. *et al.* Dehydrogenation of goethite in earth's deep lower mantle. *PNAS* **114**, 1498–1501 (2017).
152. Tang, M., Niu, Z.-W., Zhang, X.-L. & Cai, L.-C. Structural stability of FeO_2 in the pressure range of lower mantle. *J. Alloys Compd.* **765**, 271–277 (2018).
153. Huang, S. X., Wu, X. & Qin, S. Ultrahigh-pressure phase transitions in FeS_2 and FeO_2: Implications for super-earths' deep interior. *Journal of Geophysical Research-Solid Earth* **123**, 277–284 (2018).

154. Schmidt, B., Schröder, B., Sonnenberg, K., Steinhauer, S. & Riedel, S. From polyhalides to polypseudohalides: Chemistry based on cyanogen bromide. *Angew. Chem. Int. Ed. Engl.* **58**, 10340–10344 (2019).
155. Wei, S., Wang, J., Deng, S., Zhang, S. & Li, Q. Hypervalent iodine with linear chain at high pressure. *Scientific reports* **5**, 14393 (2015).
156. Zhu, Q., Oganov, A. R. & Zeng, Q. Formation of stoichiometric CsF_n compounds. *Scientific Reports* **5**, 7875 (2015).
157. Shamp, A., Saitta, P. & Zurek, E. Theoretical predictions of novel potassium chloride phases under pressure. *Phys. Chem. Chem. Phys.* **17**, 12265–12272 (2015).
158. Zhang, W. *et al.* Stability of numerous novel potassium chlorides at high pressure. *Scientific reports* **6**, 26265 (2016).
159. Guerette, M. *et al.* Advanced synthesis of Na_4Si_{24}. *Mrs Advances* **3**, 1427–1433 (2018).
160. Hohmann, E. Silicides and germanides of the alkali metals. *Z. Anorg. Allg. Chem.* 257 113–126 (1948).
161. Witte, J. The behavior of alkali metals relative to semimetals XI, the crystal structure of NaSi and NaGe. *Z. anorg. allg. Chem.* **327**, 260–273 (1964).
162. Goebel, T., Prots, Y. & Haarmann, F. Refinement of the crystal structure of tetrasodium tetrasilicide, Na_4Si_4. *Zeitschrift für Kristallographie - New Crystal Structures* **223**, 187–188 (2014).
163. Shi, J. *et al.* Investigation of new phases in the Ba-Si phase diagram under high pressure using ab initio structural search. *Phys. Chem. Chem. Phys.* **18**, 8108–8114 (2016).
164. Gao, G., Ashcroft, N. W., Miao, M. & Hoffmann, R. Novel Si networks in the Ca/Si phase diagram under pressure. *J. Phys. Chem. C* **118**, 25167–25175 (2014).
165. Li, W. *et al.* Crystal structures of $CsSi_6$ at high pressures. *Comput. Mater. Sci.* **150**, 144–148 (2018).
166. McMahan, A. K. & Albers, R. C. Insulating nickel at a pressure of 34 TPa. *Phys. Rev. Lett.* **49**, 1198–1201 (1982).
167. Parker, L. J., Atou, T. & Badding, J. V. Transition element-like chemistry for potassium under pressure. *Science* **273**, 95–97 (1996).
168. Takemura, K., Shimomura, O. & Fujihisa, H. Cs_{VI}: A new high-pressure polymorph of cesium above 72 GPa. *Phys. Rev. Lett.* **66**, 2014–2017 (1991).
169. Ahuja, R., Eriksson, O. & Johansson, B. Theoretical high-pressure studies of Cs metal. *Phys. Rev. B* **63**, 014102 (2001).
170. Zhu, Q. *et al.* Stability of xenon oxides at high pressures. *Nat. Chem.* **5**, 61–65 (2013).
171. Dewaele, A. *et al.* Synthesis and stability of xenon oxides Xe_2O_5 and Xe_3O_2 under pressure. *Nat. Chem.* **8**, 784–790 (2016).
172. Brock, D. S. & Schrobilgen, G. J. Synthesis of the missing oxide of xenon, XeO_2, and its implications for earth's missing xenon. *J. Am. Chem. Soc.* **133**, 6265–6269 (2011).
173. Dmochowski, I. Xenon out of its shell. *Nat. Chem.* **1**, 250 (2009).
174. Hermann, A. & Schwerdtfeger, P. Xenon suboxides stable under pressure. *J. Phys. Chem. Lett.* **5**, 4336–4342 (2014).
175. Feng, J., Hennig, R. G., Ashcroft, N. W. & Hoffmann, R. Emergent reduction of electronic state dimensionality in dense ordered Li-Be alloys. *Nature* **451**, 445–448 (2008).
176. Miao, M., Botana, J., Pravica, M., Sneed, D. & Park, C. Inner-shell chemistry under high pressure. *Jpn. J. Appl. Phys.* **56**, 05FA10 (2017).

177. Pauling, L. The formulas of antimonic acid and the antimonates. *J. Am. Chem. Soc.* **55**, 1895–1900 (1933).
178. Bartlett, N. Xenon hexafluoroplatinate (V) $Xe^{+}PtF_6$. *Proceedings of the Chemical Society of London* (1962).
179. Grochala, W. Atypical compounds of gases, which have been called 'noble'. *Chem. Soc. Rev.* **36**, 1632–1655 (2007).
180. Wang, X., Andrews, L., Riedel, S. & Kaupp, M. Mercury is a transition metal: The first experimental evidence for HgF_4. *Angew. Chem. Int. Ed. Engl.* **46**, 8371–8375 (2007).
181. Riedel, S., Straka, M. & Kaupp, M. Validation of density functional methods for computing structures and energies of mercury (IV) complexes. *Phys. Chem. Chem. Phys.* **6**, 1122–1127 (2004).
182. Riedel, S., Straka, M. & Kaupp, M. Can weakly coordinating anions stabilize mercury in its oxidation state +IV? *Chemistry* **11**, 2743–2755 (2005).
183. Moock, K. & Seppelt, K. Indications of cesium in a higher oxidation state. *Angew. Chem. Int. Ed. Engl.* **28**, 1676–1678 (1989).
184. Jehoulet, C. & Bard, A. J. On the electrochemical oxidation of $Cs^{\oplus}$ and other alkali-metal ions in liquid sulfur dioxide and acetonitrile. *Angew. Chem. Int. Ed. Engl.* **30**, 836–838 (1991).
185. Rahm, M., Cammi, R., Ashcroft, N. W. & Hoffmann, R. Squeezing all elements in the periodic table: Electron configuration and electronegativity of the atoms under compression. *J. Am. Chem. Soc.* **144**, 10253-10271 (2019).
186. Tramsek, M. & Zemva, B. Synthesis, properties and chemistry of xenon(II) fluoride. *Acta Chim. Slov*. **53**, 105-116 (2006).
187. Christe, K. O. *et al.* The pentafluoroxenate(IV) anion, XeF_5^-: The first example of a pentagonal planar AX_5 species. *J. Am. Chem. Soc.* **113**, 3351–3361 (1991).
188. Dronskowski, R. & Bloechl, P. E. Crystal orbital hamilton populations (COHP): Energy-resolved visualization of chemical bonding in solids based on density-functional calculations. *The Journal of Physical Chemistry* **97**, 8617–8624 (1993).
189. Silvi, B. & Savin, A. Classification of chemical bonds based on topological analysis of electron localization functions. *Nature* **371**, 683–686 (1994).
190. Rogachev, A. Y., Miao, M., Merino, G. & Hoffmann, R. Molecular CsF_5 and CsF_2^+. *Angew. Chem.* **127**, 8393–8396 (2015).
191. Goesten, M. G., Rahm, M., Bickelhaupt, F. M. & Hensen, E. J. M. Cesium's off-the-map valence orbital. *Angew. Chem. Int. Ed. Engl.* **56**, 9772–9776 (2017).
192. Miao, M. S. *et al.* Anionic chemistry of noble gases: Formation of Mg-NG (NG = Xe, Kr, Ar) compounds under pressure. *J. Am. Chem. Soc.* **137**, 14122–14128 (2015).
193. Botana, J., Brgoch, J., Hou, C. & Miao, M. Iodine anions beyond -1: Formation of Li_nI (n = 2-5) and its interaction with quasiatoms. *Inorg. Chem.* **55**, 9377–9382 (2016).
194. Li, X. *et al.* Stable lithium argon compounds under high pressure. *Scientific reports* **5**, 16675 (2015).
195. Liu, Z., Botana, J., Miao, M. S. & Yan, D. D. Unexpected Xe anions in $XeLi_n$ intermetallic compounds. *Epl* **117**, 26002 (2017).
196. Li, P., Gao, G., Wang, Y. & Ma, Y. Crystal structures and exotic behavior of magnesium under pressure. *J. Phys. Chem. C* **114**, 21745–21749 (2010).
197. Dye, J. L. Compounds of alkali metal anions. *Angew. Chem. Int. Ed. Engl.* **18**, 587–598 (1979).

198. Zurek, E. Alkali metals in ethylenediamine: A computational study of the optical absorption spectra and NMR parameters of $[M(en)_3^{\delta+}M^{\delta-}]$ ion pairs. *J. Am. Chem. Soc.* **133**, 4829–4839 (2011).
199. Jansen, M. Effects of relativistic motion of electrons on the chemistry of gold and platinum. *Solid State Sciences* **7**, 1464–1474 (2005).
200. Karpov, A., Nuss, J., Wedig, U. & Jansen, M. Cs_2Pt: A platinide(-II) exhibiting complete charge separation. *Angew. Chem. Int. Ed.* **42**, 4818–4821 (2003).
201. Yang, G., Wang, Y., Peng, F., Bergara, A. & Ma, Y. Gold as a *6p*-element in dense lithium aurides. *J. Am. Chem. Soc.* **138**, 4046–4052 (2016).
202. Brgoch, J. & Hermus, M. Pressure-stabilized Ir^{3-} in a superconducting potassium iridide. *J. Phys. Chem. C* **120**, 20033–20039 (2016).
203. Dawes, S. B., Ward, D. L., Huang, R. H. & Dye, J. L. First electride crystal structure. *J. Am. Chem. Soc.* **108**, 3534–3535 (1986).
204. Dye, J. L. *et al.* Cavities and channels in electrides. *J. Am. Chem. Soc.* **118**, 7329–7336 (1996).
205. Dye, J. L. Electrides: Early examples of quantum confinement. *Acc. Chem. Res.* **42**, 1564–1572 (2009).
206. Takemura, K. *et al.* Phase stability of highly compressed cesium. *Phys. Rev. B* **61**, 14399–14404 (2000).
207. Zurek, E., Jepsen, O. & Andersen, O. K. Muffin-tin orbital wannier-like functions for insulators and metals. *ChemPhysChem* **6**, 1934–1942 (2005).
208. Maksimov, E. G., Magnitskaya, M. V. & Fortov, V. E. Non-simple behavior of simple metals at high pressure. *Phys.-Usp.* **48**, 761 (2005).
209. Schnering, H. G. von & Nesper, R. How nature adapts chemical structures to curved surfaces. *Angew. Chem. Int. Ed. Engl.* **26**, 1059–1080 (1987).
210. Neaton, J. B. & Ashcroft, N. W. On the constitution of sodium at higher densities. *Phys. Rev. Lett.* **86**, 2830–2833 (2001).
211. Neaton, J. B. & Ashcroft, N. W. Pairing in dense lithium. *Nature* **400**, 141–144 (1999).
212. Rousseau, B. & Ashcroft, N. W. Interstitial electronic localization. *Phys. Rev. Lett.* **101**, 046407 (2008).
213. Marqués, M. *et al.* Optical and electronic properties of dense sodium. *Phys. Rev. B* **83**, 184106 (2011).
214. Gatti, M., Tokatly, I. V. & Rubio, A. Sodium: A charge-transfer insulator at high pressures. *Phys. Rev. Lett.* **104**, 216404 (2010).
215. Matsuoka, T. & Shimizu, K. Direct observation of a pressure-induced metal-to-semiconductor transition in lithium. *Nature* **458**, 186–189 (2009).
216. Pickard, C. J. & Needs, R. J. Dense low-coordination phases of lithium. *Phys. Rev. Lett.* **102**, 146401 (2009).
217. Adebayo, G. A. Ab initio calculations of optical properties of Li and K at high pressures. *J. Phys. Chem. Solids* **74**, 1221–1226 (2013).
218. Guillaume, C. L. *et al.* Cold melting and solid structures of dense lithium. *Nat. Phys.* **7**, 211–214 (2011).
219. Jin, X. *et al.* Crossover from metal to insulator in dense lithium-rich compound CLi_4. *PNAS* **113**, 2366 (2016).
220. Marques, M. *et al.* Crystal structures of dense lithium: A metal-semiconductor-metal transition. *Phys. Rev. Lett.* **106**, 095502 (2011).

221. Pickard, C. J. & Needs, R. J. Aluminium at terapascal pressures. *Nat. Mater.* **9**, 624–627 (2010).
222. Martinez-Canales, M., Pickard, C. J. & Needs, R. J. Thermodynamically stable phases of carbon at multiterapascal pressures. *Phys. Rev. Lett.* **108**, 045704 (2012).
223. Zhu, Q., Oganov, A. R. & Lyakhov, A. O. Novel stable compounds in the Mg-O system under high pressure. *Phys. Chem. Chem. Phys.* **15**, 7696–7700 (2013).
224. Dong, X. & Oganov, A. R. Electrides and their high-pressure chemistry. *Correlations in Condensed Matter under Extreme Conditions: A tribute to Renato Pucci on the occasion of his 70th birthday* (eds. Angilella, G. G. N. & La Magna, A.) 69–84 (2017).
225. Modak, P. & Verma, A. K. Pressure induced multi-centre bonding and metal–insulator transition in $PtAl_2$. *Phys. Chem. Chem. Phys.* **21**, 13337–13346 (2019).
226. Naumov, I. I. & Hemley, R. J. Origin of transitions between metallic and insulating states in simple metals. *Phys. Rev. Lett.* **114**, 156403 (2015).
227. Lv, J., Wang, Y., Zhu, L. & Ma, Y. Predicted novel high-pressure phases of lithium. *Phys. Rev. Lett.* **106**, 015503 (2011).
228. Sternheimer, R. On the compressibility of metallic cesium. *Phys. Rev.* **78**, 235–243 (1950).
229. Miao, M. S. & Hoffmann, R. High-pressure electrides: The chemical nature of interstitial quasiatoms. *J. Am. Chem. Soc.* **137**, 3631–3637 (2015).
230. Miao, M. S., Hoffmann, R., Botana, J., Naumov & Hemley, R. J. Quasimolecules in compressed lithium. *Angew. Chem. Int. Ed. Engl.* **56**, 972–975 (2017).
231. Saunders, M. *et al.* Incorporation of helium, neon, argon, krypton, and xenon into fullerenes using high pressure. *J. Am. Chem. Soc.* **116**, 2193–2194 (1994).
232. Grochala, W. A metastable He-O bond inside a ferroelectric molecular cavity: $(HeO)(LiF)_2$. *Phys. Chem. Chem. Phys.* **14**, 14860–14868 (2012).
233. Hogness, T. R. & Lunn, E. G. The ionization of hydrogen by electron impact as interpreted by positive ray analysis. *Phys. Rev.* **26**, 44–55 (1925).
234. Miao, M. Helium chemistry: React with nobility. *Nat. Chem.* **9**, 409–410 (2017).
235. Liu, Z. *et al.* Reactivity of He with ionic compounds under high pressure. *Nat. commun.* **9**, 951 (2018).
236. Botana, J. & Miao, M. Helium shows new chemistry not seen anywhere else. *Chemistry* **2**, 466–467 (2017).
237. Gao, H., Sun, J., Pickard, C. J. & Needs, R. J. Prediction of pressure-induced stabilization of noble-gas-atom compounds with alkali oxides and alkali sulfides. *Physical Review Materials* **3**, 015002 (2019).
238. Liu, H. Y., Yao, Y. S. & Klug, D. D. Stable structures of He and H_2O at high pressure. *Phys. Rev. B* **91**, 014102 (2015).
239. Bai, Y. *et al.* Electrostatic force driven helium insertion into ammonia and water crystals under pressure. *Commun. Chem.* **2**, 1–7 (2019).
240. Pickard, C. J. & Needs, R. J. Highly compressed ammonia forms an ionic crystal. *Nat. Mater.* **7**, 775–779 (2008).
241. Liu, C. *et al.* Multiple superionic states in helium–water compounds. *Nat. Phys.* **15**, 1065-1070 (2019).
242. Zhang, J. *et al.* Rare helium-bearing compound FeO_2He stabilized at deep-earth conditions. *Phys. Rev. Lett.* **121**, 255703 (2018).
243. Fredrickson, D. C. DFT-chemical pressure analysis: Visualizing the role of atomic size in shaping the structures of inorganic materials. *J. Am. Chem. Soc.* **134**, 5991–5999 (2012).

244. Hubert, H. *et al.* Icosahedral packing of B_{12} icosahedra in boron suboxide (B_6O). *Nature* **391**, 376 (1998).
245. Deng, N., Yang, G., Wang, W. & Qiu, Y. Structural transitions and electronic properties of sodium superoxide at high pressures. *RSC Advances* **6**, 67910–67915 (2016).
246. Morito, H., Momma, K. & Yamane, H. Crystal structure analysis of $Na_4Si_{4-x}Ge_x$ by single crystal X-ray diffraction. *Journal of Alloys and Compounds* **623**, 473–479 (2015).
247. Bader, R. Atoms in molecules: A quantum theory. (Oxford University Press, 1990).
248. Stillinger, F. H. Exponential multiplicity of inherent structures. *Phys. Rev. E* **59**, 48–51 (1999).
249. Zurek, E. The Pressing role of theory in studies of compressed matter. in *Handbook of Solid State Chemistry* 571–605 (2017).
250. Jansen, M. Conceptual inorganic materials discovery – a road map. *Adv. Mater.* **27**, 3229–3242 (2015).
251. Schön, J. C., Doll, K. & Jansen, M. Predicting solid compounds via global exploration of the energy landscape of solids on the ab initio level without recourse to experimental information. *Physica Status Solidi B* **247**, 23–39 (2010).
252. Revard, B. C., Tipton, W. W. & Hennig, R. G. Structure and stability prediction of compounds with evolutionary algorithms. *Prediction and Calculation of Crystal Structures: Methods and Applications* (eds. Atahan-Evrenk, S. & Aspuru-Guzik, A.) 181–222 (2014).
253. Oganov, A. R. Modern methods of crystal structure prediction. (John Wiley & Sons, 2011).
254. Lonie, D. C. & Zurek, E. XtalOpt: An open-source evolutionary algorithm for crystal structure prediction. *Comput. Phys. Commun.* **182**, 372–387 (2011).
255. Avery, P., Toher, C., Curtarolo, S. & Zurek, E. XtalOpt version r12: An open-source evolutionary algorithm for crystal structure prediction. *Comput. Phys. Commun.* **237**, 274–275 (2019).
256. Goedecker, S. Minima hopping: An efficient search method for the global minimum of the potential energy surface of complex molecular systems. *J. Chem. Phys.* **120**, 9911–9917 (2004).
257. Amsler, M. & Goedecker, S. Crystal structure prediction using the minima hopping method. *J. Chem. Phys.* **133**, 224104 (2010).
258. Laio, A. & Parrinello, M. Escaping free-energy minima. *PNAS* **99**, 12562–12566 (2002).
259. Schön, J. C. & Jansen, M. First step towards planning of syntheses in solid-state chemistry: Determination of promising structure candidates by global optimization. *Angew. Chem. Int. Ed. Engl.* **35**, 1286–1304 (1996).
260. Kirkpatrick, S., Gelatt, C. D. & Vecchi, M. P. Optimization by simulated annealing. *Science* **220**, 671–680 (1983).